frontiers | Frontiers in Catalysis

REVIEW
published: 06 April 2022
doi: 10.3389/fctls.2022.839072

A Review on Bismuth Oxyhalide (BiOX, X=Cl, Br, I) Based Photocatalysts for Wastewater Remediation

Xincong Lv, Frank Leung Yuk Lam and Xijun Hu**

Department of Chemical and Biological Engineering, The Hong Kong University of Science and Technology, Kowloon, Hong Kong SAR, China

Solar energy transformation over semiconductor-based photocatalysis is an ideal solution to environmental problems and future sustainability. Layered bismuth oxyhalides (BiOX, X = Cl, Br or I) are very attractive and promising photocatalysts in the environment fields. This review summarizes recent advances on the design of BiOX to enhance energy converting efficiency. Especially, the emerging techniques to enhance the photocatalytic behaviors of BiOX are discussed, including non-metal/metal doping, heterojunction engineering, carbon interfacing, coupling with noble metals, defect engineering, and morphology tuning. The application of BiOX composites in wastewater remediation is also reviewed in terms of organic photocatalytic oxidation and heavy metal ion photocatalytic reduction. Finally, the future chances and challenges of BiOX photocatalysts for practical application are summarized. In all, this review well underlies the innovative preparation of BiOX products for environment-related purposes.

Keywords: bismuth oxyhalide, photocatalysis, strategies for photoactivity enhancement, charge separation, wastewater remediation

OPEN ACCESS

Edited by:
Maria Olea,
University of Cambridge,
United Kingdom

Reviewed by:
Jun Di,
Nanjing University of Science and Technology, China
Seema Garg,
Amity University, India

****Correspondence:***
Frank Leung Yuk Lam
kefrank@ust.hk
Xijun Hu
kexhu@ust.hk

Specialty section:
This article was submitted to Heterogeneous Catalysis, a section of the journal Frontiers in Catalysis

Received: *19 December 2021*
Accepted: *10 March 2022*
Published: *06 April 2022*

Citation:
Lv X, Lam FLY and Hu X (2022) A Review on Bismuth Oxyhalide (BiOX, X=Cl, Br, I) Based Photocatalysts for Wastewater Remediation. Front. Catal. 2:839072. doi: 10.3389/fctls.2022.839072

INTRODUCTION

Water pollution and unavailability of clean and inexpensive water are among the biggest challenges of the 21st century (Qu et al., 2013). Water shortage attacks 1/3 of the global population, and clean drinking water is inaccessible to one billion people (WHO/UNICEF Joint Monitoring Programme for Water Supply and Sanitation and UNICEF, 2005). The remarkable enhancement in living standards since the industrial revolution increases both the demand for freshwater and the amount/variety of polluting chemicals in water (Tollefson, 2011; Richardson, 2012; Carlsen et al., 2013). The existence of emerging contaminants, including toxic heavy metal ions, antibiotics, and endocrine disrupting chemicals (Fatta-Kassinos et al., 2011; Bueno et al., 2012), in water resources made the EU Commission Services establish a new guidance on environmental quality criteria to guarantee the quality of drinking water and to preserve the aquatic environment. Among the existent technologies for water and wastewater treatment, the most common methods include adsorption, membranes, chemical oxidation, and biological treatments. However, these technologies are relatively inefficient in eliminating emerging and persistent organic compounds. The advanced oxidation processes (AOPs) based on *in situ* formation of largely reactive species (HO• and O^{2-}•) can convert organic contaminants into less harmful substances (e.g., CO_2 and H_2O) (Lee and Park, 2013). Various AOPs such as photochemical oxidation (UV/O_3 and UV/H_2O_2), chemical oxidation (O_3 and Fenton reagents), and heterogeneous photocatalysis (UV/TiO_2) (Hidalgo et al., 2007; Malato et al., 2007) are available for wastewater processing. Among the most explored and economical AOPs, photocatalysis needs only light energy without extra chemicals and runs at mild pressure and temperature (Lin et al.,

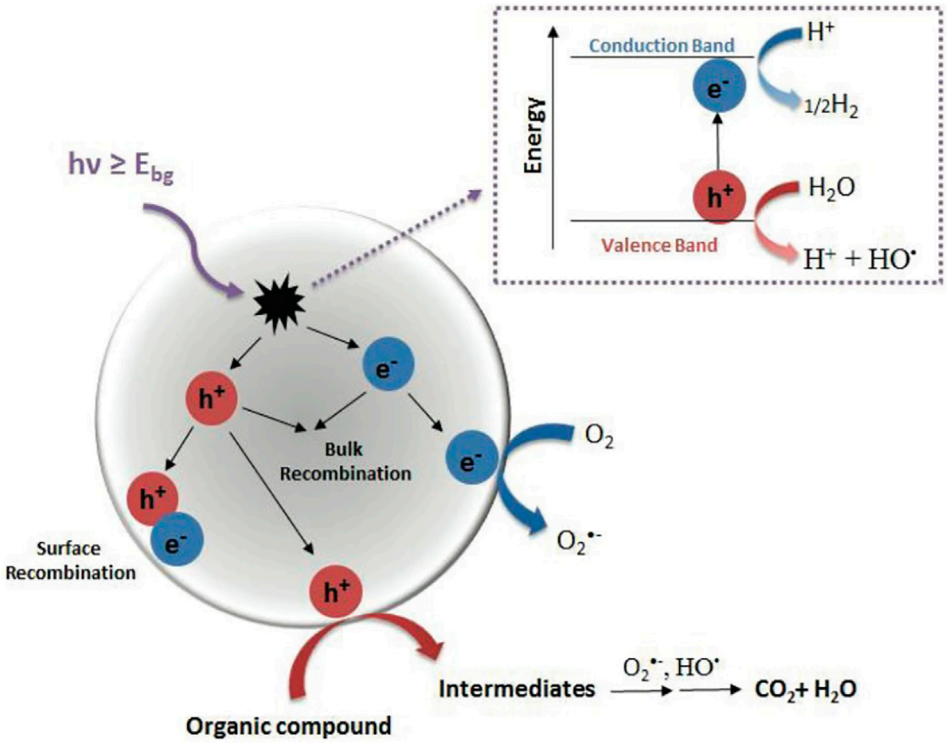

FIGURE 1 | Schematic map of the photocatalysis mechanism over an organic contaminant in water (Linsebigler et al., 1995).

2015; Landge et al., 2021). Semiconductor materials are by far the most common form of photocatalysts since they can be photoexcited by photons of energy equal to or above the bandgap energy to produce charge carriers for surface redox reactions. The overall process of photocatalysis takes five steps (Herrmann, 1999; Herrmann, 2005):

1) mass migration of reactants from the bulk medium to the catalyst–fluid interfacial region;
2) surface adsorption of the reactants;
3) photocatalyst activation and surface reaction:
   a absorption of photons by the catalyst
   b generation of electron-hole (e^--h^+) pairs
   c diffusion of photogenerated charges to the surface and
   d surface transfer of the photocharges to the reactants (i.e., surface reaction)
4) product desorption from the photocatalyst surface; and
5) mass migration of the products from the interface to the bulk fluid.

In particular, for a semiconductor photocatalyst, when irradiated light arrives at its valance band (VB), a VB electron is excited to the conduction band (CB), forming electron-hole pairs. Most of the photocharges that fail to transport away very quickly will recombine. The photocharges can also be trapped by various bulk and surface sites during the diffusion to the surface. As a result, only a fraction of the photocharges will arrive at the surface to catalyze redox reactions (Hoffmann et al., 1995). **Figure 1** displays all the reactions on the catalyst surface mentioned above.

Common photocatalysts (e.g., ZnO and TiO_2) (Raizada et al., 2016) mostly can degrade organic pollutants in water under UV irradiation (<5% solar spectrum), but their applications are limited by the low light-gathering ability, fast photocharge carrier recombination, and narrow feasible range of pH. Therefore, photocatalysts driven by visible light (~43% of solar light) with wide pH tolerance and fast division of photocharge carriers are needed. Recently, bismuth-based photocatalysts such as Bi_2O_3 (Gadhi et al., 2016; Jalalah et al., 2015; Oudghiri-Hassani et al., 2015), Bi_2WO_6 (Fu et al., 2005; Zhang and Zhu, 2005; Zhang et al., 2009), $BiVO_4$ (Yu and Kudo, 2006; Luo et al., 2011), Bi_2MoO_6 (Bi et al., 2007; Zhang et al., 2010), $BiPO_4$ (Pan and Zhu, 2011; Pan and Zhu, 2010), $Bi_2Ti_2O_7$ (Yao et al., 2004), $(BiO)_2CO_3$ (Ni et al., 2016), BiOCOOH (Xiong et al., 2011a), and bismuth oxyhalides (BiOX, X = Cl, Br, I) (Henle et al., 2007; Huang and Zhu, 2008; Huizhong et al., 2008; Zhang et al., 2008; Chang et al., 2010; Chen et al., 2013; Cheng et al., 2014; Ye et al., 2014; Yang et al., 2018) have been used in visible-light–driven water purification. Especially, BiOX with its chemical inertness, photocorrosion tolerance, and harmlessness in aqueous media has received wide attention. The BiOX becomes crystals in matlockite (PbFCl-type) tetragons (space group P4/*nmm*). The crystal lattice comprises $[Bi_2O_2]^{2+}$ slice interlayers between halogen anion dual-slabs, gathering along the *z*-axis by the nonbonding (van der Waals) interaction (**Figure 2A**) (Chen et al., 2013). This two-dimensional layered structure of BiOX

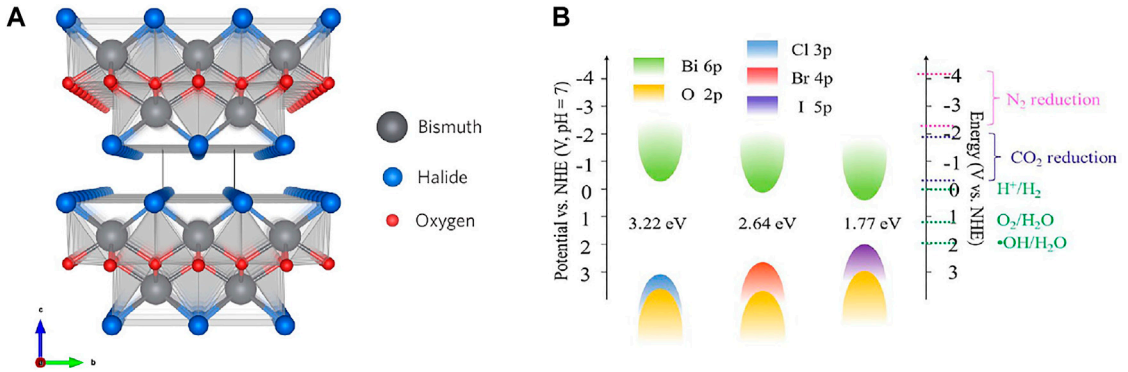

FIGURE 2 | (A) Crystal structures of BiOX (X = Cl, Br, I) (modified with permission (Ganose et al., 2016)). **(B)** Schematic VB and CB structures of BiOX (data from Ref (Guo et al., 2021)).

facilitates the formation of an inner electric field between halogen and $[Bi_2O_2]^{2+}$ slabs owing to the transformation of photoexcited electron-hole pairs (Zhang et al., 2006). The VB of BiOX is constituted by X p (X = Cl, Br or I) orbitals and O 2p orbitals (Tu et al., 2012; Zhang et al., 2012; Zhao et al., 2013) while the CB comprises Bi 6p orbitals (Cao J. et al., 2012; Zhang et al., 2013). Density functional theory (DFT) calculation indicates the distance between two slabs is elongated with the rise of the halogen atom count, following the narrowed bandgap, such as BiOCl (~3.2 eV) (Ma Z. et al., 2017), BiOBr (~2.6 eV) (Li K. L. et al., 2014; Kong et al., 2016), and BiOI (~1.8 eV) (Xiao and Zhang, 2010; Ye et al., 2011) (**Figure 2B**). Thereby, the light absorbing range can be prolonged from ultraviolet to visible light.

In 2006, Zhang *et al.* prepared the BiOCl using the hydrolysis method, and for the first time, they found that BiOCl had a better performance than TiO_2 (P25, Degussa) on photocatalytic degradation of methyl orange (MO) dye (Zhang et al., 2006). In addition, Zhang and co-workers synthesized hierarchical BiOCl nanoplate microspheres using the one-pot solvothermal method. The as-obtained BiOCl showed 1.7 times higher photocatalytic activity than TiO_2 toward MO degradation (Zhang et al., 2008). In 2015, Ding et al. prepared the BiOCl hierarchical microsphere (2–50 nm) through controlling pH in the reaction precursor, and the samples showed a preferable photocatalytic activity for rhodamine B (RhB) dye degradation (Ding et al., 2015). Although BiOCl has better performance than TiO_2, the large band gap energy (~3.2 eV) limited their application under visible light.

BiOBr had a narrower band gap (~2.6 eV) than BiOCl and thus has been used under visible irradiation in recent years. Zhang et al. prepared the BiOBr microspheres using the ethylene glycol (EG) assisting solvothermal method (Zhang et al., 2008). Due to the narrow band gap of BiOBr, it shows 2.5 times and 3.5 times higher catalytic activity than TiO_2 under UV and visible light irradiation. In addition, the flower-like hierarchical architectures of BiOBr was prepared by Jia *et al.*, who employed tetrabutylammonium halide as halogen sources in ethanol solvent (Jia et al., 2015). The as-obtained BiOBr can degrade rhodamine B and salicylic acid under visible light.

The BiOI owned the narrowest band gap energy (~1.8 eV) in BiOX and thus had the best performance under visible light in principle. However, the significant recombination of photocharges in pristine BiOI limited their photocatalytic activity. The BiOI hierarchical nanospheres show a better adsorption (57.4% removal) on MO dye than photocatalytic activity (~42.6% removal) (Li R. et al., 2015). Therefore, the BiOI was always used as light harvesting for extending the light adsorption of composites. For example, Zhang et al. prepared the TiO_2/BiOI p-n junction by using the hydrothermal-solvothermal route. The light absorption of composites can be extended to the visible region, and the separation efficiency of photocharges in TiO_2 can be improved. As a result, the TiO_2/BiOI composites show 16.6 times higher methylene blue degradation than TiO_2 (Zhang Y. et al., 2021).

Although the favorable bandgap can be obtained by changing halogen atoms, the photocatalytic ability of pristine BiOX is still inefficient due to the fast electron-hole recombination and the decreased redox ability (Guo et al., 2021). In other words, BiOX can hardly keep responsive light sensitivity, rapid carrier movement, and high redox capability at the same time.

Many methods can be used to restrict charge carrier recombination in BiOX during heterogeneous photocatalysis. One common way is to decorate BiOX materials with another semiconductor to form type II heterojunctions, such as Bi_2WO_6 (Meng and Zhang, 2015; Xiang et al., 2016; Wang F. et al., 2018; Wang J. et al., 2019; Tahmasebi et al., 2019), TiO_2 (Park et al., 2012; Yang J. et al., 2014; Choi et al., 2016; Yao et al., 2020), and Cu_2O (Cao et al., 2015; Zhang Y. et al., 2020a). Another strategy is the deposition of noble metals: the generally lower Fermi energy of metal nanoparticles than that of BiOX promotes electron migration from the semiconductor to the metal *via* Schottky contact. The most common decorative metals include platinum (Pt), silver (Ag), and gold (Au) owing to their noble and/or catalytic properties (Yu et al., 2013; Gao et al., 2014; Bi et al., 2016; Liu et al., 2018; Zhou S. et al., 2019; Yadav et al., 2021). They all function as electron sinks/reservoirs, spatially isolating the electrons from the VC photoholes of BiOX, and as more-active sites and co-catalysts for photocatalytic reduction.

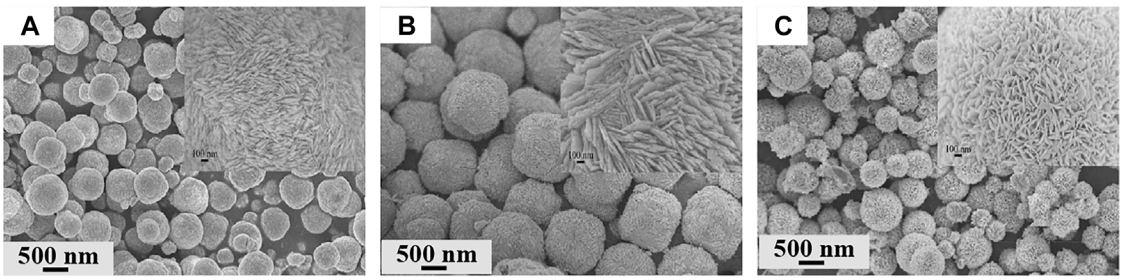

FIGURE 3 | SEM images of BiOCl **(A)**, BiOBr **(B)**, and BiOI microspheres **(C)** (reproduced with permission (Zhang et al., 2008)).

Another useful method for extracting photoelectrons from BiOX to prevent charge carrier recombination is to prepare composites with carbon materials, particularly graphene-based nanomaterials (Chou et al., 2016; Dai and Zhao, 2017; Lee et al., 2017; Garg et al., 2018a; Su et al., 2018; Sharma N. et al., 2019; Zhang W. et al., 2019; Zhu et al., 2019; Yadav et al., 2020; Alansi et al., 2021; Sharma et al., 2022). Because of the fast electron motion in graphene, photoelectrons from the CB of BiOX to graphene are easily isolated from the BiOX surface. The other methods including defect engineering, Bi-rich strategy, morphology, and thickness control have also been reported and summarized in various review studies (Di et al., 2017; Li et al., 2018; Xiong et al., 2020). However, few studies focus on the intuitive comparison of photocatalytic activity of BiOX prepared by different methods for wastewater treatment.

Herein, we summarize recent advances in BiOX photocatalysts for wastewater remediation. First, we briefly probe into the preparation schemes for BiOX, which is regarded as essential from the application perspective. Then, various strategies to improve BiOX photocatalytic activity are discussed, such as facet management, element doping, heterojunction, defect engineering, and Schottky barriers. After that, the behaviors, decomposition routes of representative organics, and probable mechanisms during degradation by bismuth catalysts are assessed. Last, the problems of BiOX-based photocatalytic processes in water environmental use are listed.

SYNTHETIC METHODS OF BIOX PHOTOCATALYSTS

Hydro/Solvothermal Method

The hydro/solvothermal method is the most widely used for producing diverse micro/nanostructured BiOX. Specifically, a chemical reaction proceeds in a sealed pressure vessel at high temperature and pressure in water or an organic solvent. The products often possess high crystallinity without calcination. Huo *et al.* prepared BiOBr nanosheets by hydrothermally treating $Bi(NO_3)_3{\cdot}5H_2O$ and KBr at 160°C for 12 h (Li K. L. et al., 2014). A similar procedure was extended to the preparation of BiOCl (Xiong et al., 2011b) and BiOI (Li H. et al., 2013). Different from the hydrothermal route which uses a precursor water solution, the solvothermal route adopts various solvents (e.g., methanol (Vadivel et al., 2014), ethylene glycol (Liu et al., 2014), and glycerol (Liu Z. et al., 2012)) to synthesize the precursor solution. This route allows the increment of pressure and temperature relative to the hydrothermal route (Liu Z. et al., 2012). Zhang *et al.* first produced 3D BiOX microspheres by using the solvothermal route with ethylene glycol (**Figure 3**) (Zhang et al., 2008) Furthermore, difference in solvents during this route impacts the growing direction of BiOX crystals. Xiong et al. studied the effect of alcohol chain length on the thermal preparation of BiOBr by using methanol, n-butanol, and n-hexanol as solvents at 180°C for 5 h in a stainless steel vessel (Xiong et al., 2016). When the carbon chain length of n-alcohol was prolonged, the characteristic diffraction peaks of BiOBr at the (102) and (110) facets were sharper and stronger, indicating the improvement of BiOBr crystallization.

The adoption of precursors during preparation directly affects the BiOX facets. As reported, BiOBr with exposed (001) facet is photocatalytically more active, because the (001) facet has much lower surface energy than other facets and BiOBr materials have an intraelectric field along the [001] direction (Zhao et al., 2012). The use of ionic liquid Br instead of KBr led to the generation of BiOBr with exposed (001) facet, because the ionic liquid is passivating and can lower the facet surface energy (Mao et al., 2014).

The addition of surfactants such as polyvinylpyrrolidone (PVP) and hexadecyl-trimethyl-ammonium bromide can reportedly regulate morphology. Liu et al. made BiOBr flower-nanospheres with 32.9 m^2/g surface area *via* the solvothermal procedure using $Bi(NO_3)_3{\cdot}5H_2O$, PVP (M = 45,000~58,000), bromide $[C_{16}min]Br$, and ethylene glycol as precursors while keeping the reaction at 140°C for 24 h (Liu and Wu, 2017). Hao *et al.* compared the effect of PVP on BiOI photocatalytic activity (Hao et al., 2012). With PVP, the BiOI nanosheets self-aggregated to form 3D hierarchical microspheres, which exhibited a higher photocatalytic activity in tetracycline hydrochloride (TCHC) degradation than 2D-BiOI nanoplates (removal rate 94 vs. 44%).

Alcoholysis/Hydrolysis

Both hydrolysis and alcoholysis methods offer mild conditions for synthesis of BiOX, but the products have nonuniform dimensions. For instance, BiOCl nanostructures were synthesized from 6 h of $BiCl_3$ hydrolysis at 65°C using acetylacetone as an assisting solvent under acidic conditions

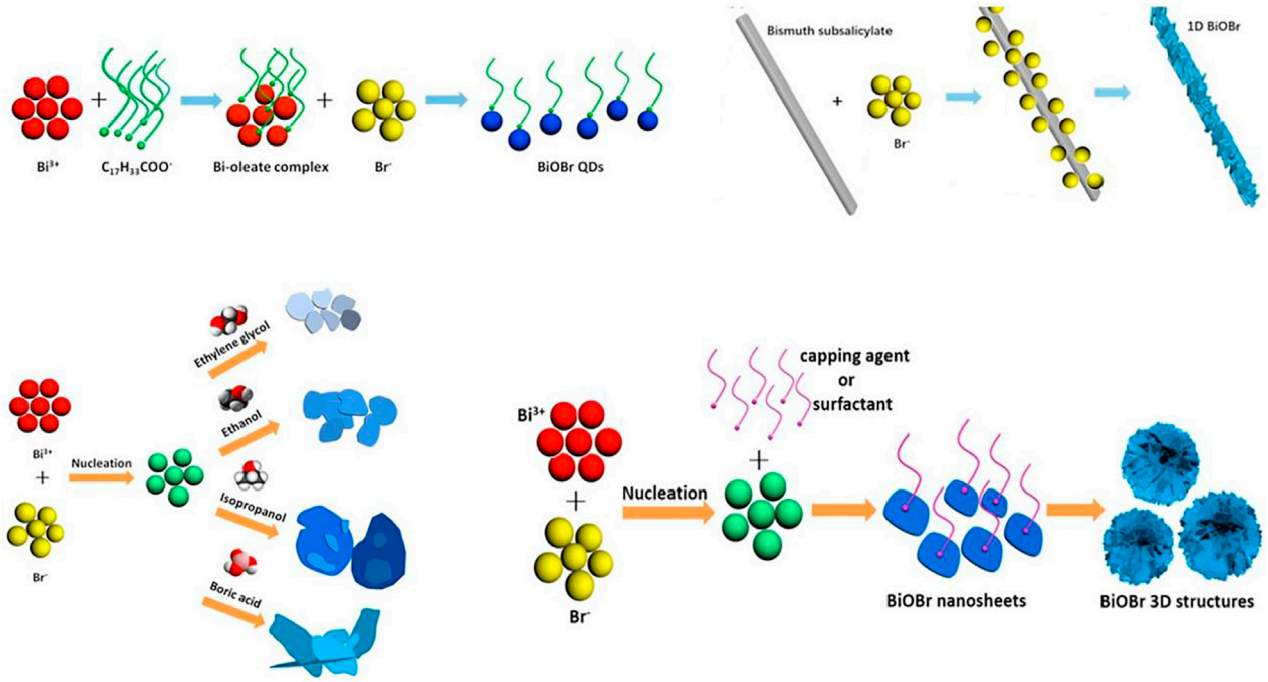

FIGURE 4 | Schematic map of the probable formation of 0D, 1D, 2D, or 3D BiOBr (Modified from Ref (Han et al., 2020)).

(Armelao et al., 2012). Song et al. prepared 21- to 85-nm-thick BiOCl nanosheets from hydrolysis of $Bi(NO_3)_3$ with HCl and Na_2CO_3 by keeping it at ~ pH2 for 30 min at ambient temperature (Song et al., 2017). Zhang et al. compared the photocatalytic activity of BiOBr prepared by hydrolysis and alcoholysis and added 0.5 g of $BiBr_3$ to 15 ml of solvent of water or isopropyl alcohol at room temperature (Li R. et al., 2015). Then the suspension was heated at 20, 40, or 60°C for 10 min, and the pH was kept at 9. The BiOBr from hydrolysis was nanosheet-shaped and composed of the best crystallinity and unique (102) facets, while the BiOBr from alcoholysis was flower-like with exposed (110) facets. Both showed a superior photocatalytic activity toward methyl orange (MO) degradation, but the BiOBr from hydrolysis had higher photostability after 4 cycles. Huang et al. prepared BiOBr with different shapes (0D spherical quantum dots, 1D nanorods, 2D nanosheets, and 3D hierarchical architectures) through room-temperature hydrolysis (**Figure 4**) (Han et al., 2020) Different bismuth or bromine sources, solvents, capping agents, or surfactants affected the morphology of BiOBr during hydrolysis. The direct hydrolysis of BiI_3 was used to prepare BiOI by Su et al., who used the as-obtained BiOI to degrade Rhodamine B under simulated solar light (Su et al., 2014).

Template Method

This method alters the morphology of BiOX mainly by modulating the crystal nucleation and growth during the synthesis. Nanomaterial synthesis by the template method basically takes three steps (Xie et al., 2016). 1) A template is produced. 2) The target product is synthesized under the action of the template *via* precipitation, sol-gel, hydrothermal, or other common synthetic method. 3) The template is removed. Cui et al. adopted carbonaceous microspheres as a template to adsorb Bi^{3+} and Cl^{-}, followed by sintering up to 400°C to form hollow BiOCl microspheres, which were in a shell thickness of 40 nm and a diameter of 200 nm (Cui et al., 2016). With a butterfly wing as a biological template, Yan et al. prepared hierarchical BiOCl (Yan et al., 2019). BiOI was also used as a self-sacrifice template to construct $Bi_4O_5I_2/Bi_5O_7I$ and $BiOI/Bi_4O_5I_2$ heterojunctions from simple calcination (Cheng et al., 2020). The BiOBr self-sacrifice template was also used for the formation of $BiOBr/Bi_4O_5Br_2$ (Li P. et al., 2020).

Other Methods

Microwave, co-precipitation, and calcination can also be used to synthesize BiOX. For example, Chen et al. prepared BiOBr with a 3D flower-like structure after 27 min of microwave processing (Li et al., 2012). The BiOBr showed a Brunauer, Emmett and Teller (BET) surface area of 63.5 m^2/g and an outstanding removal ability and fast adsorbing rate over Cr^{6+} in a wide pH range. Reportedly, the presence of surfactants during microwave processing improved the BiOBr photocatalytic activity (Chen et al., 2017). The BiOCl was also prepared by microwave with the same procedure as BiOBr and showed an excellent visible-light photocatalytic activity for dye Rhodamine B (RhB) (He et al., 2015). Ai et al. prepared the hierarchical porous BiOI using the microwave method. The as-obtained BiOI shows an excellent adsorption ability toward Congo red in water and it can be easily regenerated under light irradiation (Ai et al., 2014).

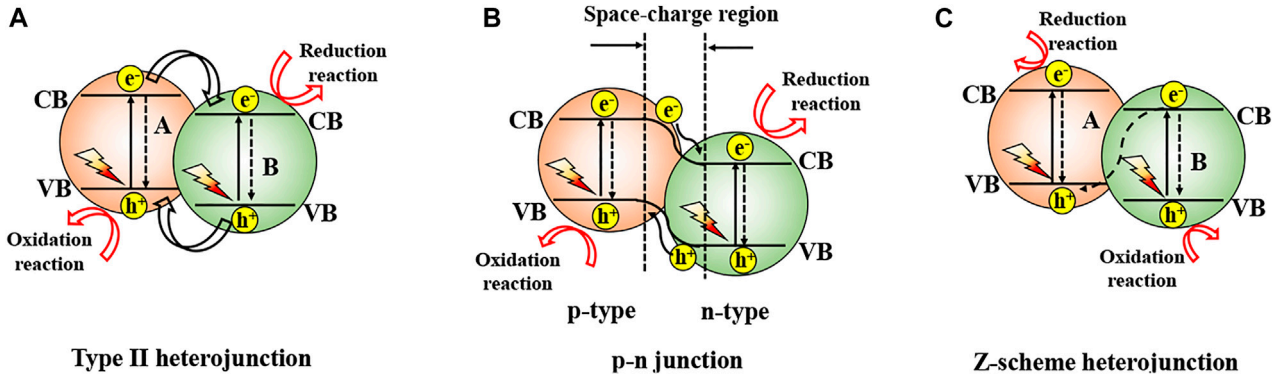

FIGURE 5 | (A) Type II photocatalysts; **(B)** p-n junction; and **(C)** Z-scheme strategy for higher photocatalytic activity.

During preparation of BiOBr by co-precipitation (Lu et al., 2012), $Bi(NO_3)_3$ and KBr were mixed in acetic acid water solution, stirred, and aged for 6 h. The BiOCl microflowers were successfully prepared by using a simple co-precipitation method, and it had a better photocatalytic activity under acidic conditions than neutral and alkaline conditions (Wang and Zhang, 2020). The BiOI was also prepared by co-precipitation and EDTA was introduced as the retarder of the reaction and a structure-directing agent in aqueous media. The as-obtained BiOI exhibited a large BET surface area (~47.5 $m^2\ g^{-1}$) and thus had an excellent photocatalytic activity for NO removal (98%) in the gaseous phase (Montoya-Zamora et al., 2017).

The unstable halogen atoms in BiOX can easily escape due to the weak van der Waals forces. Therefore, phase transformation can be achieved by directly heating BiOX. Plate-like $Bi_{24}O_{31}Br_{10}$ was prepared *via* sintering of BiOBr at 750°C (Yu C. et al., 2012). A similar process was extended to the synthesis of hollow $Bi_{24}O_{31}Cl_{10}$ microspheres at 600°C (Cui et al., 2016). The 3D hierarchical bismuth oxyiodides was prepared using the ethylene glycol–assisted *in situ* hydrolysis method and the subsequent calcination at high temperature. The multiform bismuth oxyiodides obtained at different temperatures exhibit very distinct microstructure and band structure, and their photoabsorption was tuned from 700 to 400 nm in an orderly manner, rendering the adjustable oxidation and reduction ability of band energy levels (Huang et al., 2017).

VARIOUS TECHNIQUES TO IMPROVE PHOTOCATALYTIC ACTIVITY OF BIOX

Like any semiconductor-mediated photocatalysis, the maximum efficiency is decided by charge separation/transportation and surface catalytic performance. Inappropriate use of photoelectrons with low thermodynamic energy due to the presence of a positive CB will deteriorate the charge isolation of BiOBr and BiOI. Although BiOCl has a more negative CB, the large bandgap (~3.22 eV) limits its application under visible light. Therefore, to enhance the visible light and photocatalytic capabilities of BiOX, diverse approaches like heterojunction, metal/nonmetal doping, noble metal deposition, interfacing with carbon materials, defect engineering, etc. can be adopted to strengthen the organic photodegradation efficiency.

Heterojunction

Heterojunction basically refers to the band alignment caused by the interface between two types of semiconductors with unequal band structures. Heterojunction is divided by the band positions of the semiconductors into three types (Yang, 2021). Type II, the most widely used one, offers the best band positions for effective charge carrier isolation, which results in higher photocatalytic activity. The photoelectrons will be transported from the CB of semiconductor A to the CB of semiconductor B for favorable energetics of the relative positions of the CBs (**Figure 5A**). Holes are transferred at the same time from the VB of semiconductor B to the VB of semiconductor A. Under light illumination, the electrons and holes are spatially isolated from each other, lowering the recombination possibility (Ning et al., 2016). Yang et al. prepared type II Bi_2WO_6/BiOBr heterojunction *via* a one-step solvothermal route for degradation of rhodamine B (RhB), methylene blue, and colorless TCHC (**Figure 6A**) (Ren et al., 2019) Guo et al. prepared $BiVO_4$/BiOCl heterojunction with a higher charge separation rate than pure $BiVO_4$ or BiOCl (Liu et al., 2019). More research on BiOX-based Type II heterojunction can be found in **Table 1**.

Though type-II heterojunction can perfectly isolate electrons-holes in space, the improvement in such isolation across this heterojunction is unable to prevent the ultrafast hole-electron recombination on the semiconductor. Therefore, p-n junction is proposed for greatly effective charge acquisition and isolation. Generally, p- and n-type semiconductors upon contact will constitute a p-n junction with an interfacial space-charge zone due to the electron and hole diffusion and thus generate a built-in electrical potential that can guide the electron and hole migration in the opposite direction (**Figure 5B**) (Jiang L. et al., 2012; Li L. et al., 2014; Jiang and Li, 2015) When incident light with an energy at least equal to the bandgap values irradiates the p-n junction, both p- and n-type semiconductors can be excited to form electron-hole pairs (Lin et al., 2011; Cao J. et al., 2012; Peng et al., 2014). The electrons are stimulated by the electric field to

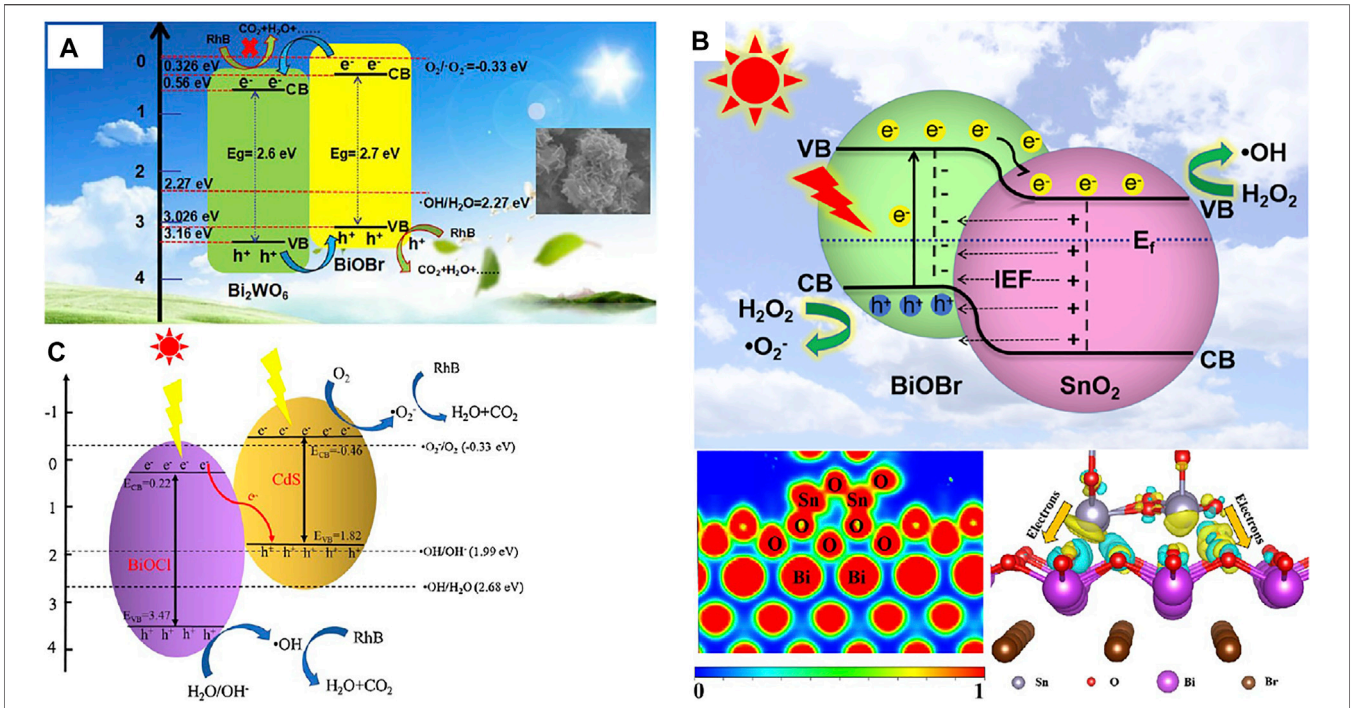

FIGURE 6 | (A) Photocatalytic mechanism of pollution by Bi_2WO_6/BiOBr catalyst (Type II heterojunction) (Ren et al., 2019). **(B)** Diagram of BiOBr/SnO_2 p-n heterojunction charge transfer at the interface, electron location function, and charge difference distribution (Wu et al., 2020); **(C)** Charge transfer in Z-scheme CdS/BiOCl catalyst (Tang et al., 2020).

move to the CB of the n-type semiconductor, and the holes to the VB of the p-type semiconductor. Consequently, the electron-hole pairs are separated in p-n heterojunctions more quickly than in type-II heterojunctions due to the cooperation between the inner electric field and band arrangement (Yu et al., 2010). Wang et al. prepared p-type BiOBr and interfaced with n-type $Bi_2O_2CO_3$ by precipitation conversion. The photoactivity of BiOBr/$Bi_2O_2CO_3$ p-n junction is 14.8 folds that of bare $Bi_2O_2CO_3$ (Wang J. J. et al., 2020). Sun et al. prepared BiOBr/SnO_2 p-n heterojunctions to eliminate NO in visible light. Importantly, the charge transfer channels and directions at the BiOBr/SnO_2 interface were determined by theoretical calculations (**Figure 6B**) and experiments (using XPS) (Wu et al., 2020). Similar research was extended to BiOCl and BiOI (**Table 1**).

Although the above heterojunctions are advantageous in separating photoelectron-hole pairs, the redox ability of these systems is weakened and thus cannot provide sufficient driving force for a specific photocatalytic reaction. Direct Z-scheme heterojunction photocatalysts have been proposed for spatial division of photoelectrons and holes whilst preserving the strong redox ability of two semiconductors (**Figure 5C**). Under irradiation, the CB photoelectrons of semiconductor A with strong reducing ability and the VB holes of semiconductor B with strong oxidizing ability are preserved. The CB photoelectrons of semiconductor B with low reducing ability and the VB holes of semiconductor A with low oxidizing ability recombine. The 4% CdS/BiOCl heterojunction prepared by Lin et al (Lin et al., 2017) showed a 10% higher photoactivity than pristine BiOCl in elimination of RhB, which was due to the direct Z-scheme mechanism (**Figure 6C**). In a new Z-scheme BiOBr/$MnFe_2O_4$ nanocomposite, spontaneous transfer of photoelectron carriers contributed to the photoelectron-hole division and decelerated the electron-hole recombination (Sin et al., 2020). Other Z-scheme photocatalysts were also reported before (**Table 1**).

Elemental Doping

Incorporation of transition metal ions into BiOX lattices to generate or modify the electronic states has gained much attention. Furthermore, it may induce lattice defects in BiOX or change crystallinity to prevent electron-hole combination, forming long-lasting carriers. Doping with special metal ions can also enhance light absorption region, which remarkably influences the photoelectrochemical (PEC) performance of semiconductors. Doping with transition metal ions (e.g., Fe^{3+}, Cu^{2+}, and Mn^{3+}) will form impurity energy levels and may induce a redshift in the energy band, which is attributed to the electron transition from impurity bands to the CB or VB. Cu^{2+} was doped into BiOBr by using the solvothermal method to form the doping level (**Figure 7**), which strengthened both light absorption and electron-hole isolation efficiency (Lv et al., 2020). Consequently, the Cu^{2+}-doped BiOBr showed a 2.28 times higher visible-light–driven photocatalytic activity relative to pristine BiOBr. A similar method was used to prepare Fe^{2+}-doped BiOBr (Li W. et al., 2017). The doping of tungsten resulted in a bandgap reduction and the generation of an impurity band in the forbidden zone of BiOCl, as confirmed by first-principle

TABLE 1 | Summary of BiOX-based composites with improved photocatalytic activity.

Photocatalysts	Synthesis method	Light source	Improved performances
Heterojunction			
Bi_2WO_6/BiOBr (Ren et al., 2019) (Type II)	Solvothermal	λ ≥ 420 nm (300 W Xe lamp)	12 times that of BiOBr and 23 times that of Bi_2WO_6 for RhB degradation in 60 min
S-C_3N_4/BiOBr (Vinoth and Pandikumar, 2021) (Type II)	Ultrasonic hydrothermal	AM 1.5G, 100 mW/cm^2	13 times that of BiOBr and 89 times that of S-gC_3N_4 for PEC water oxidation
Bi_2SiO_5/BiOBr (Chai et al., 2019) (Type II)	Ion exchange	λ ≥ 420 nm (300 W Xe lamp)	1,253 times that of BiOBr and 25.2 times that of $BiVO_4$ for RhB degradation in 90 min
$BiVO_4$/BiOCl (Liu et al., 2019) (Type II)	Ion exchange	AM 1.5G, 100 mW/cm^2	102 times that of BiOCl and 1.44 times that of $BiVO_4$ for PEC water splitting
Bi_2S_3/BiOCl (Wang Y. et al., 2018) (Type II)	Epitaxial growth	λ ≥ 420 nm, 100 mW/cm^2	15 times that of BiOCl and 2 times that of Bi_2S_3 for PEC water splitting
CeO_2/BiOCl (Wang H. et al., 2020) (Type II)	Precipitation hydrothermal	λ ≥ 420 nm (300 W Xe lamp)	1.67 times that of BiOCl and 3.37 times that of CeO_2 for methyl tetracycline degradation in 120 min
g-C_3N_4/BiOI (Vinoth et al., 2021) (Type II)	Ultrasonic hydrothermal	AM 1.5G, 100 mW/cm^2	2 times that of BiOI and 11 times that of g-C_3N_4 for PEC water splitting
SnS/BiOI (Juntrapirom et al., 2017) (Type II)	Hydrothermal coprecipitation	λ ≥ 400 nm (50 W Hg lamp)	1.67 times that of BiOI and 4.97 times that of SnS for MO degradation in 60 min
BiOBr/$Bi_2O_2CO_3$ (Wang J. J. et al., 2020) (p-n junction)	Precipitation conversion	300 W Xe lamp	14.7 times that of $Bi_2O_2CO_3$ and 4.03 times that of BiOBr for RhB degradation in 20 min
BiOBr/SnO_2 (Wu et al., 2020) (p-n junction)	Hydrothermal	λ ≥ 420 nm (150 W Xe lamp)	1.5 times that of BiOBr and 12.2 times that of SnO_2 for NO removal in 5 min
$BiPO_4$/BiOCl (Zhang Z. et al., 2020) (p-n junction)	*In situ* chemical transformation	300 W xenon lamp	3.18 times that of BiOCl for RhB degradation in 90 min
BiOI/g-C_3N_4 (Tian et al., 2020) (p-n junction)	Precipitation	λ ≥ 420 nm (300 W Xe lamp)	10 times that of g-C3N4 and 4 times that of BiOI for bisphenol A degradation in 4 h
TiO_2/BiOI (Zhang Y. et al., 2021) (p-n junction)	Hydrothermal	Visible light, 300 mW/cm^2	16.6 times that of TiO_2 and 1.38 times that of BiOI for methylene blue degradation in 60 min
BiOI/ZnO (Xiao et al., 2020) (p-n junction)	Hydrothermal	λ ≥ 420 nm (300 W Xe lamp)	9.2 times that of BiOI and 2 times that of ZnO for methylene blue degradation in 180 min
CDs/BiOCl (Lin et al., 2017) (Z-scheme)	Electrochemical	λ ≥ 420 nm (350 W Xe lamp)	7.62 times that of BiOCl for RhB degradation in 180 min
BiOBr/$MnFe_2O_4$ (Sin et al., 2020) (Z-scheme)	Hydrothermal	Visible light (105 W compact fluorescent lamp)	2.85 times that of BiOBr and 6.42 times that of $MnFe_2O_4$ for RhB degradation in 80 min
BiOBr/$BiOIO_3$ (Jia et al., 2020a) (Z-scheme)	Solvothermal	λ < 400 nm (9 W LED light)	1.24 times that of $BiOIO_3$ and 4.42 times that of BiOBr for removal of heavy metal mercury in 60 min
BiOBr/Bi_2MoO_6 (Wang S. et al., 2017) (Z-scheme)	Two-step coprecipitation	λ ≥ 420 nm (300 W Xe lamp)	10.0 times that of pure BiOBr and 54.5 times that of pure Bi_2MoO_6 for RhB degradation in 25 min
AgI/BiOBr (Yu et al., 2018) (Z-scheme)	Solvothermal precipitation	λ ≥ 420 nm (300 W Xe lamp)	2.75 times that of BiOBr and 52.5 times that of AgI for ciprofloxacin degradation in 60 min
$SnNb_2O_6$/BiOCl (Jiang et al., 2019) (Z-scheme)	Two-step hydrothermal	λ ≥ 420 nm (250 W Xe lamp)	10.51 times that of $SnNb_2O_6$ and 20.58 times that of BiOCl for benzocaine degradation in 90 min
BiOCl/g-C_3N_4 (Sun et al., 2020) (Z-scheme)	Hydrothermal	Simulated solar light (300 W Xe lamp)	20.51 times that of BiOCl for tetracycline degradation in 60 min
BiOI/Bi_2O_4 (Qin et al., 2020) (Z-scheme)	Ultrasonic hydrothermal	100 W LED lamp	2.81 times that of Bi_2O_4 and 30 times that of BiOI for RhB degradation in 32 min
Co_3O_4/BiOI (Malefane et al., 2020) (Z-scheme)	Solvothermal	60 W LED lamp	80.1 times that of Co_3O_4 and 13.5 times that of BiOI for ibuprofen degradation in 60 min
Elemental doping			
Cu^{2+}-doped BiOBr (Lv et al., 2020)	Solvothermal	λ ≥ 420 nm (300 W Xe lamp)	2.28 times higher than that of undoped BiOBr for norfloxacin degradation in 90 min
Zn^{2+}-doped BiOBr (Zhou J. et al., 2019)	Solvothermal	λ ≥ 420 nm (300 W Xe lamp)	3.35 times enhancement for the RhB degradation in 30 min
Ag/Ti-doped BiOBr (Jiang G. et al., 2012)	Solvothermal reduction	λ ≥ 400 nm (11 W daylight lamp)	5.11 times enhancement for the RhB degradation in 30 min
Sn^{2+}-doped BiOBr (Tu et al., 2015)	Solvothermal	Visible light (500 W Xe lamp)	2.71 times higher than pure BiOBr for RhB degradation in 16 min
Zn^{2+}-doped BiOCl (Li W. T. et al., 2015)	Solvothermal	λ ≥ 420 nm (300 W Xe lamp)	2.71 times higher than pure BiOCl for the RhB degradation in 60 min
Mn^{3+}-doped BiOCl (Pare et al., 2011)	Hydrolysis	Visible light (500 W halogen lamp)	1.53 times improvement for malachite green photodegradation in 180 min
N-doped BiOBr (López-Velázquez et al., 2021)	Microwave-assisted solvothermal	300–800 nm with an intensity of 30 W/m^2 in the UV region	3.3, 2.2, 4.1, and 1.4 times improvement for bisphenol A, 17β-estradiol, 17α-ethinylestradiol, and 4-tert-octylphenol photodegradation, respectively

(Continued on following page)

TABLE 1 | (*Continued*) Summary of BiOX-based composites with improved photocatalytic activity.

Photocatalysts	Synthesis method	Light source	Improved performances
P-doped BiOI (Ma F.Q. et al., 2017)	Hydrothermal	λ ≥ 420 nm (300 W Xe lamp)	2.63 times higher than BiOI for RhB degradation in 60 min
C-doped BiOBr (Zhang W. et al., 2019)	Hydrothermal	λ ≥ 420 nm (800 W Xe lamp)	4.7 times enhancement for tetracycline degradation in 25 min
S-doped BiOBr (Liu et al., 2021)	Solvothermal	λ ≥ 420 nm (300 W Xe lamp)	3 times higher than pure BiOBr for ibuprofen degradation in 240 min
La^{3+}-doped BiOBr (Yin et al., 2017)	Solvothermal	λ ≥ 400 nm (300 W Xe lamp)	3.8 and 1.7 times enhancement for RhB in 60 min and ciprofloxacin in 180 min degradation, respectively
Y^{3+}-doped BiOCl (Zhong et al., 2020)	Consecutive solvent-based and thermal	Visible light (300 W xenon lamp)	1.8 times improvement for the tetracycline hydrochloride within 90 min
Er ion–doped BiOBr (Xia et al., 2016)	Solvothermal	λ ≥ 400 nm (300 W Xe lamp)	1.8-fold improvement for ciprofloxacin degradation within 360 min
Noble metal deposition			
Ag/BiOBr (Yu et al., 2011)	Photodeposition	Visible light (300-W tungsten lamp)	14-fold improvement for acid orange II degradation in 40 min
Pd/BiOBr (Li X. et al., 2020)	Photodeposition	Xe lamp at 200 mW cm^{-2}	1.5 times improvement for photocatalytic selective oxidation of toluene to benzaldehyde
Rh, Pd, Pt/BiOCl (Yu et al., 2013)	Photodeposition	420 nm < λ < 660 nm (150 W tungsten halogen lamp)	2.1, 2.2, and 3.1 times enhancement for Rh, Pd, and Pt deposited BiOCl for acid orange II degradation
Ag/BiOCl (Yu et al., 2017)	Photodeposition	Two 365 nm LED lamps with an average light intensity of 80 mW cm^{-2}	2.5-fold improvement for MO degradation
Pd/BiOCl (Chen et al., 2014)	Solvothermal	Visible light (300 W Xe lamp)	2.5-fold enhancement for RhB degradation
Au/BiOI (Chang et al., 2021)	Ion sputter	AM 1.5G at 100 mW/cm^2 (300 W Xe lamp)	24-fold improvement in PEC efficiency over bare BiOI
Ag/BiOI (Liu H. et al., 2012)	Hydrothermal and photodeposition	λ ≥ 420 nm (500 W Xe lamp)	4.00, 3.99, and 3.39 times improvement over BiOI in degradation of acid orange II, MO, and RhB, respectively
Interfacing with carbon materials			
BiOBr/graphene (Tu et al., 2012)	EG-assisted solvothermal	λ ≥ 420 nm (500 W Xe lamp)	3 times higher than BiOBr for RhB degradation
BiOBr/graphene hydrogel (Chang et al., 2020)	Two-step hydrothermal	Visible light (300 W Xe lamp)	1.83 times higher than that of BiOBr for degradation of potassium butyl xanthate
BiOCl/graphene (Li Z. et al., 2017)	Hydrothermal	Full arc (150 W Xe lamp)	8.4 and 3.8 times higher than BiOCl for degradation of MO and oxidation of water
GO foam/BiOI	*In situ* deposition	λ ≥ 400 nm (60 W LED spotlight lamp)	1.84 times improvement for phenol degradation in 150 min
BiOI/CNT (Sharma et al., 2021)	Hydrothermal	Visible light (4 × 24 W visible light lamps)	2 times and 3 times higher than BiOI for degradation of phenol and RhB
BiOI-MWCNT (Su et al., 2012)	EG-assisted solvothermal	λ ≥ 400 nm (150 W Xe lamp)	2.1 times higher than BiOI for degradation of acid orange II in 180 min
BiOCl-carbon quantum dots (Di et al., 2015)	Mannitol-assisted solvothermal	λ ≥ 400 nm (300 W Xe lamp)	2.22 and 2.12 times higher than pure BiOCl for the degradation of RhB in 40 min and degradation of BPA in 120 min
Defect engineering			
BiOBr-OV (Li H. et al., 2015)	EG-assisted solvothermal	λ ≥ 420 nm (LED light, 10 W/cm^2)	Can generate NH_3 under light irradiation versus BiOBr without OV
BiOBr-OV (Lyu et al., 2019)	Solvothermal	Full arc (10 W LED lamp)	3.5 times improvement for tetracycline degradation over BiOBr
OV-rich S-doped BiOBr (Wang Q. et al., 2019)	Solvothermal	λ ≥ 420 nm (300 W Xe lamp)	4.9 and 18.0 times those of pristine BiOBr and OV-poor S-doped BiOBr for 4-CP degradation within 120 min
BiOBr-OV (Shi et al., 2018)	Solvothermal	Visible light (300 W Xe lamp)	3, 2.69, 2, and 1.74 times improvement for degradation of phenol, BPA, RhB, and MO compared with OV-poor BiOBr, respectively
$BiO_{1-x}Cl$ (Cao et al., 2018)	Diethylene glycol solvothermal	λ ≥ 400 nm (300 W Xe lamp)	Adsorbing 42% ciprofloxacin and 40% doxycycline, no adsorption on BiOCl; degrading ciprofloxacin and doxycycline after 40 min, only 30% removal over BiOCl
BiOCl-OV (Song et al., 2021)	Sodium dodecylbenzenesulfonate hydrothermal	λ ≥ 400 nm (Xe lamp)	1.48 times improvement for the oxytetracycline hydrochloride degradation
BiOCl-OV (Cui et al., 2018)	Solvothermal	λ ≥ 420 nm (300 W Xe lamp)	3.3 times higher for oxygen evolution than OV-poor BiOCl
BiOI-OV (Huang et al., 2014)	Solvothermal	λ ≥ 420 nm (500 W Xe lamp)	1 order-of-magnitude improvement in donor density versus BiOI and 10 times higher photocatalytic activity than BiOI for MO degradation

(Continued on following page)

TABLE 1 | (*Continued*) Summary of BiOX-based composites with improved photocatalytic activity.

Photocatalysts	Synthesis method	Light source	Improved performances
BiOI-OV (Chen et al., 2016)	Glycerol solvothermal	Visible light (300 W Xe lamp)	3.5 times higher than untreated BiOI nanosheets for MO degradation
Facet control			
BiOBr-110 (Peng et al., 2017)	Glucose hydrothermal	λ ≥ 400 nm (300 W Xe lamp)	Degrading 91% MO in 30 min and 100% RhB in 10 min, 60% MO and 70% RhB by BiOBr-001
BiOBr-010 (Wu et al., 2017)	Chemical precipitation	Visible light (300 W Xe lamp)	3 times improvement of PEC performance over BiOBr-001
BiOBr-010 (Jia et al., 2020b)	pH adjustment	λ < 420 nm (9 W LED lamp)	1.2 times improvement for Hg oxidation over BiOBr-001
BiOCl-001, BiOCl-010 (Jiang J. et al., 2012)	Hydrothermal	UV or visible light (300 W Xe lamp)	UV: 1.6 times enhancement for MO degradation in BiOCl-001 over BiOCl-010; visible light, 2.5 times higher in BiOCl-010 versus BiOCl-001
Thickness tuning			
Thickness-controllable $Bi_{24}O_{31}Br_{10}$ nanosheets (Wang C. Y. et al., 2017)	NH_4Br hydrothermal	λ ≥ 420 nm (520 W Xe lamp)	$Bi_{24}O_{31}Br_{10}$ (~40 nm thickness) is 3.11 and 4.79 times higher than that of $Bi_{24}O_{31}Br_{10}$ with 80 nm and with 130 nm thickness for tetracycline hydrochloride degradation
Morphology control			
BiOI hollow microspheres (Di et al., 2014)	Ionic liquid-assisted microemulsion method	λ ≥ 400 nm (300 W Xe lamp)	BiOI hollow microspheres are 4 times higher than BiOI nanosheets for degradation of RhB in 150 min
$Bi_{12}O_{17}Br_2$ nanotubes (Di et al., 2020)	Solvothermal treatment	300 Xe lamp	$Bi_{12}O_{17}Br_2$ nanotubes, exhibiting 14.4 times higher activity than $Bi_{12}O_{17}Br_2$ nanoplates for CO_2 photoreduction

theoretical computation and experimental findings. (Yang W. et al., 2014). Other commonly used transitional metal dopants reported in BiOX include Zn^{2+} (Li J. et al., 2015; Zhou et al., 2019b), Ti^{4+} (Jiang G. et al., 2012), Al^{3+} (Weng et al., 2014a), Sn^{4+} (Tu et al., 2015), and Mn^{3+} (Pare et al., 2011).

The incorporation of non-metal dopants can distribute extra extrinsic electronic levels in the band gap, which greatly affects light adsorption and charge carrier isolation. The main hypothesis is that the VB shifts upward to its maximum level after valence orbitals and local states hybridize from valence orbitals (Chen et al., 2015). Many non-metals such as N, Fen-Qiang Ma et al. (2017), Zhancheng Zhang et al. (2019), Obeid et al. (2020), Liu et al. (2021), and López-Velázquez et al. (2021) were doped into BiOX to improve the photocatalytic activity. Wang *et al.* prepared the boron-doped BiOBr nanosheets, in which the B dopants form an impurity level to accelerate charge separation (**Figure 7G**) (Wu et al., 2016) Carbon doping can enhance the internal electric field of Bi_3O_4Cl and thereby increase bulk-charge separation to 80% (Li et al., 2015). This homogeneous carbon-doped Bi_3O_4Cl was prepared by using a glucose-hydrothermal method, followed by thermal treatment to allow the diffusion of the carbon dopant in host lattices. A similar method was employed by Jin *et al.* to prepare C-doped $Bi_{24}O_{31}Cl_{10}$ from oxytetracycline hydrochloride as a carbon and chlorine source (Jin et al., 2018).

Rare earth metals with a 4f electron shell are rich in electronic energy levels, which function as electron trapping centers for photocharge carriers. Hence, doping with rare earth metals may promote charge separation and overall photocatalytic performance. In the La^{3+}-doped BiOBr microspheres produced by using an ionic liquid ([C16mim] Br)-assisted solvothermal route, (Yin et al., 2017), the substitution of Bi^{3+} by La^{3+} was monitored by XRD peak shift, while no La_2O_3 or another phase of La was found. The La-doped BiOBr significantly increased the photodegradation of ciprofloxacin, which was because La may trap photoelectrons and thus inhibit the electron-hole recombination (**Figures 7H–J**). Similarly, Y-doped BiOCl improved the visible-light photocatalytic activity in tetracycline decomposition (Zhong et al., 2020). Moreover, europium and erbium were also used as dopants in BiOX recently (Xia et al., 2016).

Noble Metal Modification

Deposition of noble metals (e.g., Ag, Pt, Rh, or Pd) on the surface of BiOX to build a space-charge dividing region (namely, the Schottky barrier) is another effective method to promote photo-charge separation. At the interface between a noble metal and BiOX, the electron transfer from the higher-Fermi-level BiOX to the lower-Fermi-level metal will arrange the Fermi energy levels. The presence of the Schottky barrier endows the metal and the semiconductor with excessive negative and positive charges, respectively. The Schottky barrier also acts as an effective electron trap against electron-hole reconnection in photocatalysis, which often leads to a higher photocatalytic capability. More recently, the deposition of Ag nanoparticles (NPs) on BiOX was found to remarkably improve dye decomposition efficiency under UV or visible light illumination (Yu et al., 2011; Yu C. L. et al., 2012). Li et al. prepared Pd/BiOBr by photodeposition (**Figure 8A**) and found the existence of Pd initiated the formation of more oxygen vacancies on the surface of BiOBr due to the electron interaction at the Pd–BiOBr interface. The coexistence of Pd and oxygen vacancies on BiOBr facilitates the adsorption of O_2 and toluene molecules (**Figure 8B**). As a result, the Pd/BiOBr interface controls the charge division and

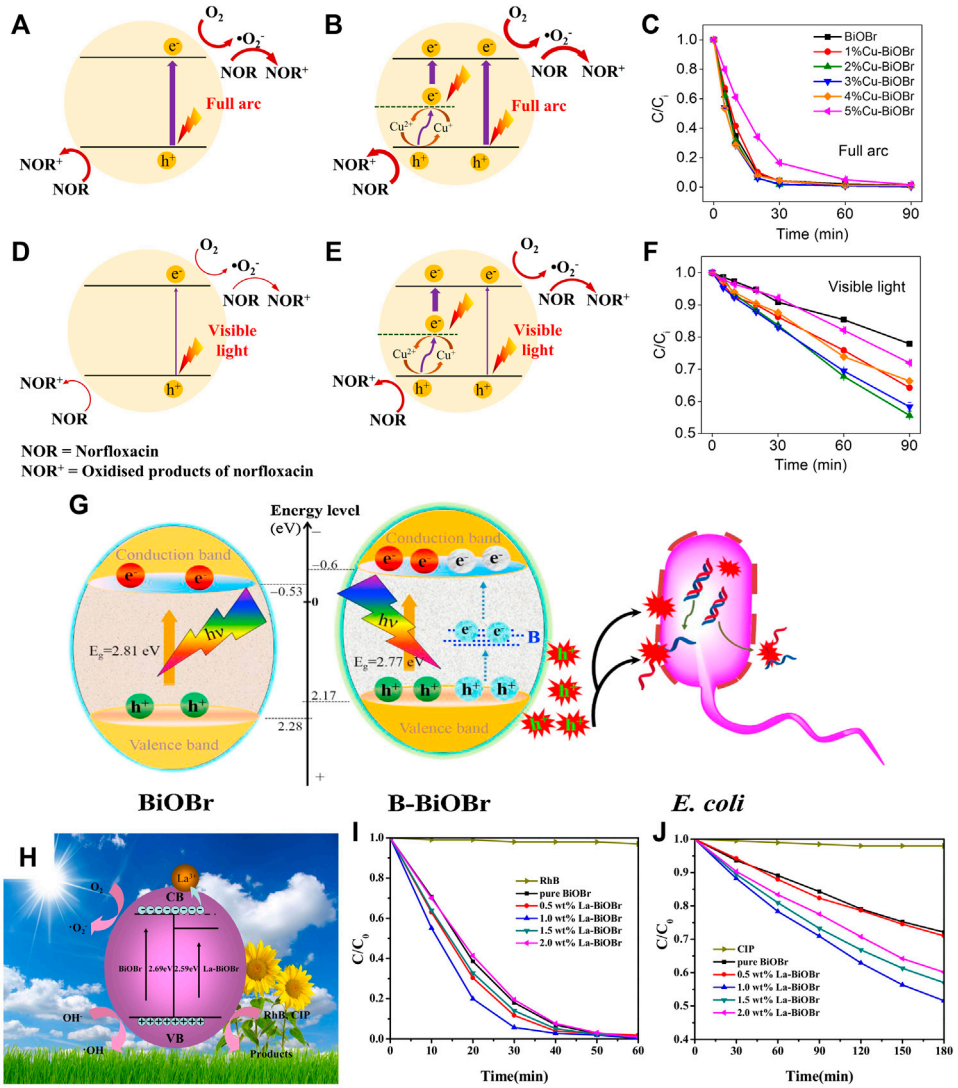

FIGURE 7 | Mechanistics of photocharge transport and surface transfer on BiOBr **(A,D)** and Cu-BiOBr **(B,E)** with norfloxacin and dissolved oxygen under full **(A,B)** arc and visible light **(D,E)** irradiation. The corresponding degradation kinetics under full arc **(C)** and visible light **(F)** (Lv et al., 2020). **(G)** Photocatalytic bacterial inactivation enhancement of B-BiOBr nanosheets (Wu et al., 2016). **(H–J)** Organic degradation over La^{3+}-doped BiOBr and corresponded degradation kinetic for RhB and CIP (Yin et al., 2017).

activates O_2 and toluene, improving the photocatalytic activity of BiOBr by 1.5 times in 99% selective oxidation of toluene to benzaldehyde (**Figure 8C**) (Li X. et al., 2020) Yu *et al.* investigated how noble metals (Rh, Pd, and Pt) deposition affected the photocatalytic behaviors of BiOX. The impact of the noble metals ranks as Pt > Pd > Rh under UV and as Rh > Pt > Pd under visible light. The noble metal NPs also function as electron traps to quicken electron-hole division and thus improve the visible light activity (Yu et al., 2013).

Interfacing with Carbon Materials

Due to the excellent electrical conductivity, flexibility, and specific surface, carbon materials are ideal supporting scaffolds for homogeneous anchoring of functional nanomaterials. Xu et al. coated hierarchical BiOX (X = Cl or I) on the newly prepared functional carbon nanotubes through ionic layer adsorption and reaction. The nanotubes with outstanding mechanical properties and pollutant absorbing ability were used to tailor the energy gaps of BiOX *via* covalent bonds (**Figure 9A**) (Weng et al., 2014b). Similarly, the BiOI/multi-walled carbon nanotube composites prepared by Xiong *et al.* using the solvothermal method photocatalytically outperformed pure BiOI owing to the interfacial charge-transfer (**Figure 9B**) (Su et al., 2012). Graphene is another common carbon material to couple with BiOX. Li et al. prepared a BiOBr/graphene composite by an *in situ* solvothermal route using graphene oxide (**Figure 9C**). The graphene oxide was reduced to graphene, and BiOBr NPs were formed on the surface. This composite has higher photocatalytic activity in degrading RhB (Tu et al., 2012). Reduced graphene oxide (RGO)/BiOCl hybrids were

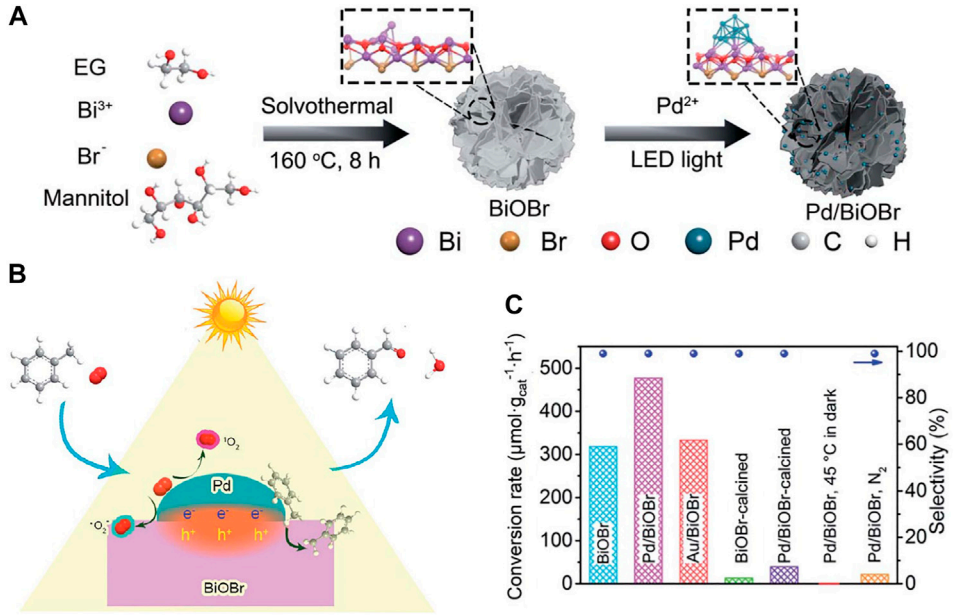

FIGURE 8 | (A) Schematic scheme for preparation of Pd/BiOBr; **(B)** photocatalytic selective toluene oxidation to benzaldehyde over Pd/BiOBr and **(C)** comparison of toluene conversion and selectivity among photocatalysts (reproduced with permission (Li X. et al., 2020)).

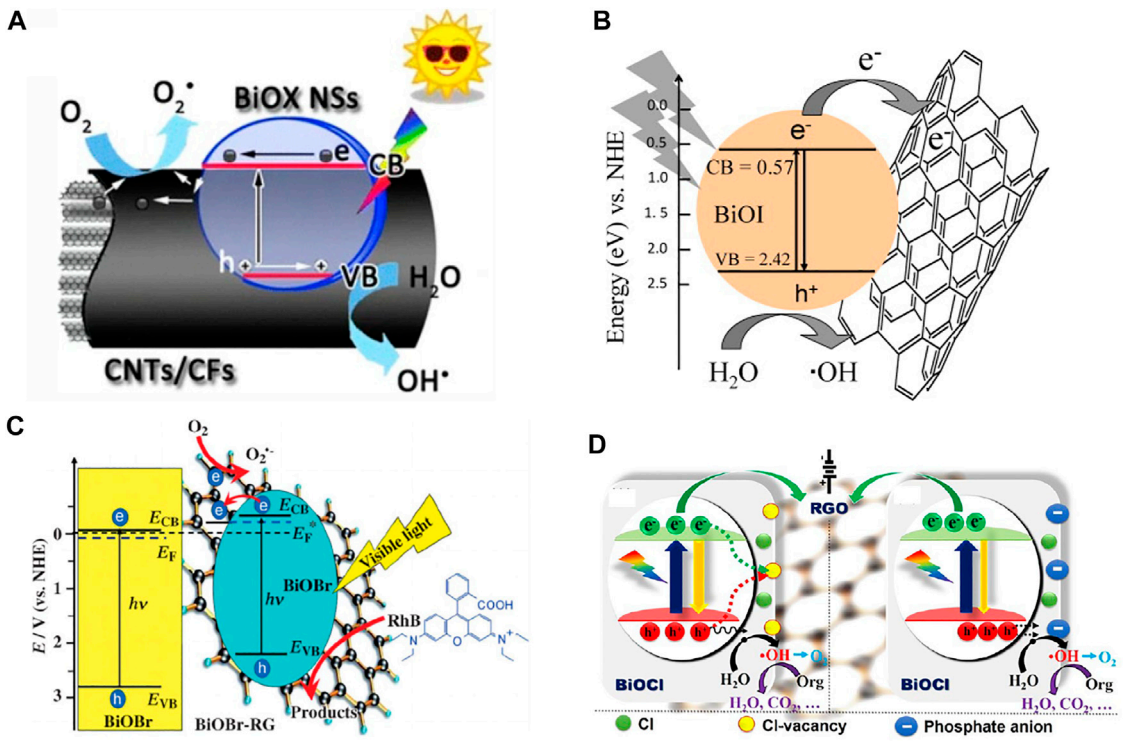

FIGURE 9 | (A) Mechanism of photocatalytic reaction over BiOX/CNT (Weng et al., 2014b). **(B)** Electron transfer between BiOI and MWCNT (Su et al., 2012). **(C)** Photodegradation over BiOBr/graphene (Tu et al., 2012). **(D)** Charge transfer of RGO/BiOCl photoanodes before and after phosphate modification (Li Z. et al., 2017) (all reproduced with permission).

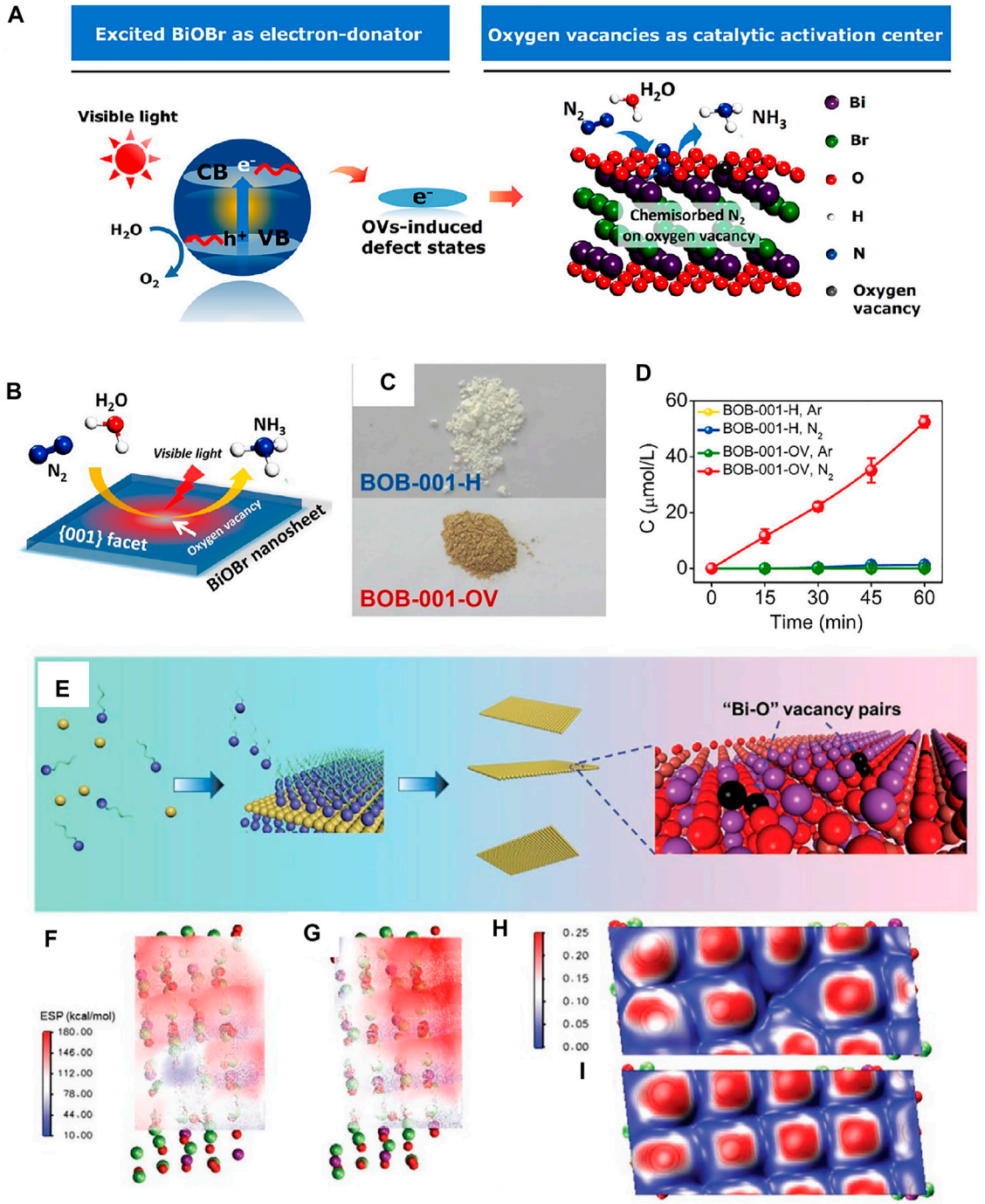

FIGURE 10 | (A) Schematic map of photocatalytic N_2 fixation over BiOBr with OV. **(B)** Photocatalytic N_2 fixation model with water as both the solvent and proton source. **(C)** Colors of BiOBr with or without OV. **(D)** Quantitative monitoring of NH_3 formed over different photocatalysts (Li et al., 2015d). **(E)** Illustration of the formation process of $Bi_{24}O_{31}Br_{10}$ with Bi-O vacancy pairs. Electrostatic potential of **(F)** $Bi_{24}O_{31}Br_{10}$ with Bi-O vacancy pairs and **(G)** perfect $Bi_{24}O_{31}Br_{10}$. Electron localization function of **(H)** $Bi_{24}O_{31}Br_{10}$ with Bi-O vacancy pairs and **(I)** perfect $Bi_{24}O_{31}Br_{10}$ (Di et al., 2021).

synthesized by Zhang et al. with graphene oxide as the precursor (Li Z. et al., 2017). The RGO/BiOCl was 8.4 and 3.8 times more photocatalytically active than BiOCl in MO degradation and water oxidation, respectively. This was because the chemical bonding of BiOCl with RGO led to faster charge separation and longer carrier lifetime. It is indicated that chloride vacancies may act as recombination centers to impede photocharge separation (**Figure 9D**). Carbon quantum dots (CQDs) with quasi-spherical nanoparticles usually <10 nm in diameter have been introduced to BiOX recently. Li *et al.*

prepared the CQD-modified BiOCl which showed the enhanced photocatalytic activity due to superior electron transfer ability of CQDs (Di et al., 2015). Furthermore, the nitrogen-doped CQD–modified BiOBr was prepared by the same group to boost the photodegradation toward ciprofloxacin, rhodamine B, tetracycline hydrochloride, and bisphenol A (Di et al., 2016).

Defect Engineering

The creation of defects permits the adjustment of micro/electron structure, atom coordination number, and charge transfer in BiOX. Zhang et al. prepared the [001] facet exposed BiOBr with oxygen vacancy (OV) by using an ethylene glycol–assisted solvothermal method and used it to fix atmospheric N_2 to NH_3 (**Figures 10A,B**) (Li et al., 2015d). The sample without OV was also synthesized by further sintering in an O_2 atmosphere, and the color turned white (**Figure 10C**). NH_3 was detected over BiOBr with OV, but not in BiOBr without OV (**Figure 10D**). This was because the OV in BiOBr was the catalytic activation center and can chemisorb N_2 on the surface. Similarly, Xue et al. used BiOBr nanosheets with OV to realize N_2 to NH_3 (Xue et al., 2018). The Bi_3O_4Br nanosheets with single-unit-cell thickness and confined defects have been controllably prepared by Di et al., who demonstrated that the bismuth vacancy can greatly facilitate the generation of oxygen defects, accounting for the formed oxygen defects in the bismuth oxyhalides (Di et al., 2019). Wang et al. prepared OV-rich S-doped BiOBr by one-step solvothermal treatment. The optimal BB-5S degraded 98% 4-chlorophenol (4-CP) under visible light within 120 min, which was 18.0 and 4.9 times those of OV-poor sulfur-doped BiOBr and pristine ultrathin BiOBr, respectively. Experiments and DFT computation showed a sub-band was formed under the synergy of OVs and S doping, which largely facilitated visible-light absorption capability and inhibited photocharge recombination, thus improving photocatalytic activity (Wang Q. et al., 2019). Cui et al. solvothermally prepared OV-rich BiOCl nanosheets (Cui et al., 2018). A new energy level from OV was verified both theoretically and experimentally. BiOCl nanosheets with OV were capable of photocatalytic oxygen evolution under visible light. Additionally, OV-rich BiOCl displayed a higher visible-light photocurrent and more efficient photocharge division and migration than BiOCl with fewer OVs.

Apart from the single vacancies, the effect of surface vacancy pairs in BiOX on photocatalytic activity has been explored recently. When the thickness of BiOX decreased to atomically thin, the atomic-escape energy will be smaller and then surface atoms will escape from the 2D lattice and create vacancies more easily (Di et al., 2018a). Liu and co-workers prepared the $Bi_{24}O_{31}Br_{10}$ atomic layer with "Bi-O" vacancy pairs by a mild polyvinylpyrrolidone (PVP) self-assembly strategy coupled with pH adjusting (see **Figure 10E**). In contrast to the perfect surface, $Bi_{24}O_{31}Br_{10}$ with Bi-O vacancy pairs own large local electric field intensity (**Figures 10F,G**). Furthermore, the presence of Bi-O vacancy pairs would create an electron delocalization hot spot (**Figures 10H,I**), where both inflow and outflow of electrons are better favored. Therefore, the separated charges can be effciently delivered to target reactants, significantly enhancing the catalytic reaction rate (Di et al., 2021).

Facet Control

Semiconductor photocatalysts with specific exposed crystal surfaces can improve photo-charge separation and transportation, which further strengthens the photocatalytic performances. In general, surfactants and H^+ are used to modulate the exposed crystal surface. Glucose can be the capping and structure-directing agent in preparing one-dimensional rod-like BiOBr with exposed (110) facets (BiOBr-110) (**Figure 11A**) (Peng et al., 2017). Glucose can interact with the (001) facet of BiOBr NPs to prevent the development of these planes, leading to the generation of ultrathin BiOBr nanosheets with exposed (001) facets. In the meantime, glucose drives the ultrathin nanosheets to gather along the [001] orientation, forming BiOBr nanorods with exposed (110) facets. BiOBr-110 photocatalytically outperforms BiOBr-001 owing to the lower resistance and higher efficiency of charge transfer. Zhao *et al.* prepared the BiOCl with high ratios of [001] and (Li et al., 2012) facets (BiOCl-H1 and BiOCl-H2, respectively) under various acid conditions (**Figure 11D**) (Zhao et al., 2020), which remarkably raised the RhB photodegradation efficiency. The apparent rate constant of BiOCl-H2 was 0.0961 min^{-1}, about 2.7 times that of BiOCl-H1 (**Figures 11E,F**). The Z-scheme facet heterojunction was constructed to accelerate charge separation and transportation (**Figure 11D**). Zhang *et al.* found that single-crystal BiOCl nanosheets with exposed [001] facets were more active in direct semiconductor photoexcited MO removal under UV light, but the counterpart with exposed [010] facets was highly active in indirect dye photosensitive decomposition under visible light (Jiang J. et al., 2012).

Thickness Tuning

Thickness tuning is another strategy for improving the photocatalytic activity of BiOX. When the thickness of BiOX is reduced, the quantum confinement can be realized to tune the band edge structure, which is favorable for meeting the potential requirement of various catalytic reactions. In addition, the charge migration distance can be shortened from the inside to the surface which improves the separation efficiency of charges. Low-coordinated atoms with dangling bonds can provide active sites to participate in the catalytic reactions (Di et al., 2018b; Xiong et al., 2018). The thickness-dependent photocatalytic activity toward salicylic acid degradation was reported by Li *et al.*, who prepared the thinner and thicker Bi_3O_4Cl through the liquid phase exfoliation under isopropanol or further recrystallization (Li J. et al., 2013). The thinnest Bi_3O_4Cl endows the highest photodegradation activity due to the highest internal electric field. The thinner thickness of $Bi_{24}O_{31}Br_{10}$ was prepared when a larger amount of NH_4Br was used. The higher charge separation efficiency can be realized in thinner $Bi_{24}O_{31}Br_{10}$ nanosheets, thus leading to the formation of higher reactive oxygen species concentration, favoring the degradation of tetracycline hydrochloride (Wang C. Y. et al., 2017).

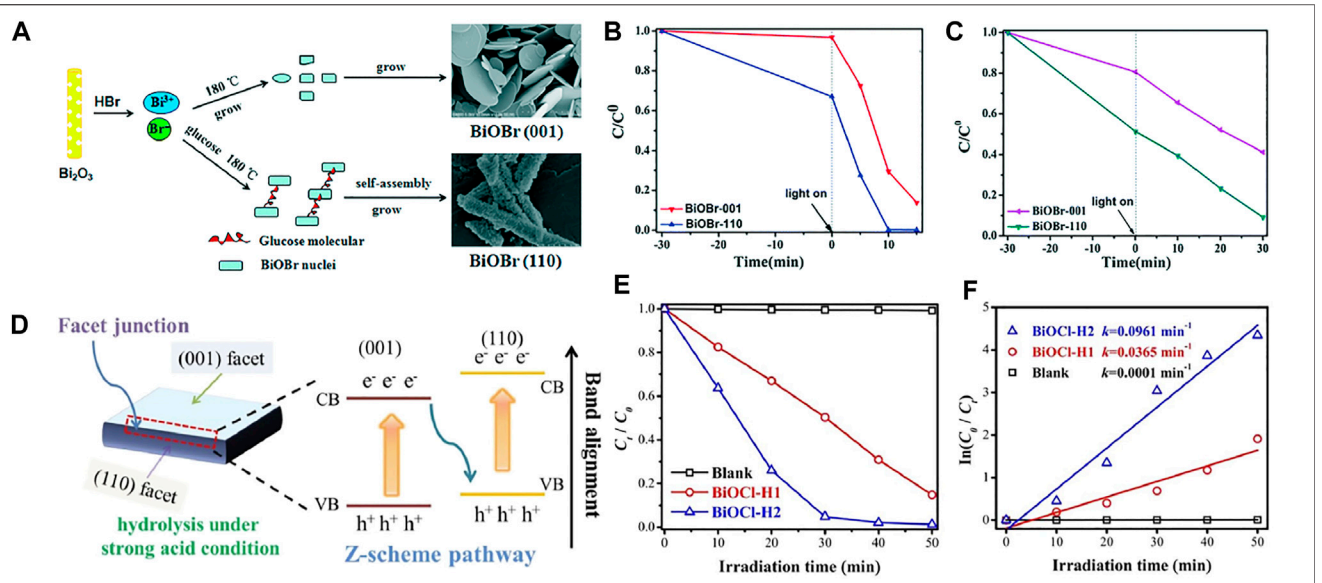

FIGURE 11 | (A) Schematic map of the proposed formation mechanism of BiOBr-110. **(B)** RhB and **(C)** MO degradation over BiOBr-110 and BiOBr-001 (Peng et al., 2017). **(D)** Facet junction interface charge transportation. **(E)** Photodegradation of RhB and **(F)** dynamic fitting by using a first-order model (Zhao et al., 2020) (all reproduced with permission).

Morphology Control

The morphology control is a classic but effective strategy for boosting the photocatalytic activity of BIOX (Garg et al., 2018b; Bárdos et al., 2019; Bárdos et al., 2020). It is well known that porous and hollow solids have excellent adsorptive properties, which is a prerequisite for highly efficiently utilizing photo-induced electron-hole pairs during photocatalysis. BiOI hollow microspheres were synthesized using a facile reactable ionic liquid 1-butyl-3-methylimidazolium iodine ([Bmim]I)-assisted microemulsion method at room temperature (Di et al., 2014). The as-obtained BiOI hollow microspheres shows enhanced photocatalytic activity, which was attributed to the shortened diffusion pathways, lower energy band gap, higher BET surface area, faster interfacial charge transfer rate, and higher separation efficiency of photogenerated electrons and holes. Liu and co-workers prepared the $Bi_{12}O_{17}Br_2$ nanotubes, exhibiting 14.4 times more activity than $Bi_{12}O_{17}Br_2$ nanoplates (Di et al., 2020). The enhanced activity is attributed to better CO_2 adsorption and activation, increased carrier separation, and CO desorption, which was induced by the surface tensile strain in $Bi_{12}O_{17}Br_2$ nanotubes.

Bismuth-Rich Strategy

By adjusting the elemental constituents, the energy band structures of BiOX materials can be tuned to meet the requirement of various applications. For example, the bismuth-rich BiOCl and BiOBr can narrow the band gap compared to pristine BiOCl and BiOBr while bismuth-rich BiOI shows an increased band gap (Li J. et al., 2017; Wang Z. et al., 2019). In addition, the bismuth-rich BiOX materials own more abundant tunable surface atomic configurations including surface atomic types, atomic quantity, and atomic distance. $Bi_{24}O_{31}Br_{10}$ materials display outstanding photocatalytic hydrogen evolution behavior, while the pristine BiOBr has been demonstrated to be inactive for photocatalytic hydrogen evolution (Shang et al., 2014).

PURIFICATION OF POLLUTANTS AND PHOTOCATALYST RECOVERY

The very positive VB and the modification of BiOX endow photoholes with sufficient thermodynamic energy to be used in organic oxidation. The organics can be degraded directly through hole-oxidation or indirectly by the newly formed oxidative radicals such as hydroxyl radicals (OH^-). During this process, the photoelectrons will be removed by dissolved oxygen to maximize the net charge separation efficiency and can also be used to reduce heavy metal ions.

Oxidation Degradation

Photooxidative degradation of many organic pollutants over modified BiOX has been extensively reviewed (Yang et al., 2018; Sharma K. et al., 2019; Garg et al., 2019). Both the decomposition mechanism and the number of intermediates depend on the properties of organic compounds. The abundant organic dyes in textile, apparel, and paper industrial wastewater cause severe environmental pollution. The dye-polluted wastewater carries refractory pigments that are highly harmful and carcinogenic to humans (Brown and De Vito, 1993; Chen et al., 2010). Dyes even at extremely low levels (below 1 ppm) are highly visible in water and severely worsen water environments (Ledakowicz and Gonera, 1999; Grzechulska and Morawski, 2002; Daneshvar et al., 2004). In general, organic dyes

are either cationic or anionic according to their chemical structures. Cationic dyes (e.g., RhB, methylene blue, and malachite green) carry cationic functional groups (mostly N^+) that can dissociate into cations in aqueous solutions. In contrast, anionic dyes including acid orange 7 and MO contain sulfonic or carboxylic acid groups. Both anionic and cationic functional groups can interact with BiOX with a hydrophilic surface, which is favorable for the oxidation by hole or hydroxyl radicals. For instance, RhB was mainly degraded by hole and hydroxyl radicals in BiOBr/BiOF (Jiang et al., 2017). However, the RhB degradation by BiOBr/TiO_2 heterojunction was mediated by superoxide radical anions (O^{2-}), which was produced by single electron reduction of dissolved oxygen (Yang et al., 2021). Organic dye degradation was also investigated using different BiOX-based photocatalysts, namely, BiOCl/CeO_2 (Zhang Y. et al., 2020b), W-doped BiOCl (Mokhtari and Tahmasebi, 2021), Bi_2WO_6/BiOX (X = Cl, Br, I) (Derikvand and Tahmasebi, 2021), and $BiVO_4$/BiOX (X = F, Cl, Br, I) (Razavi-Khosroshahi et al., 2019).

The release of antibacterial agents into the aquatic environment has caused more concerns about their potential environmental risks, especially the occurrence and spread of antibiotic resistance and chronic toxicity to microbial species. Fluoroquinolones (e.g., norfloxacin, ciprofloxacin, moxifloxacin, and ofloxacin) are extensively used as human and veterinary medicine owing to their wide-spectrum activity against Gram- and Gram-negative bacteria (Brain et al., 2004; Liu C. et al., 2012). However, fluoroquinolones cannot be fully metabolised in the body and are largely excreted in their pharmacologically active forms, which make them the most-detected antibiotics in wastewater and surface water (Robinson et al., 2005). In general, the degradation of fluoroquinolones mainly involves amine side-chain degradative oxidation, defluorination, and decarboxylation (Chen and Chu, 2015). Of them, the degradation of the electron-rich amine side-chain to oxidized products is extremely important (Sturini et al., 2012). Different BiOX-based photocatalysts were also designed to reduce antibiotics. For example, Cu^{2+}-doped BiOBr (Lv et al., 2020), Nb^{5+} -doped BiOBr (Wei et al., 2020), and N-doped BiOCl (Maimaitizi et al., 2020) were used in the degradation of norfloxacin. Type II heterojunctions such as $BiVO_4$/BiOCl (Ma X. et al., 2017), BiOBr/Fe_2O_3 (Guo et al., 2017), and BiOBr/CdS (Senasu et al., 2021) can reportedly enhance the photodegradation of antibiotics.

Apart from the oxidation degradation of organic dyes and antibiotics, modified BiOX can also be applied to other common organics, including pharmaceutical active compounds (Heidari et al., 2020; Gao et al., 2021) and endocrine-disrupting chemicals (López-Velázquez et al., 2021; Wu et al., 2021; Zhang H. et al., 2021). However, only organics transformation occurs in most cases. Therefore, future works shall focus on the development of modified BiOX with strong oxidation ability to degrade organics and mineralize their byproducts.

Reduction of Heavy Metals

Heavy metal water pollution is a global environmental problem that threatens human health and the ecology. Hexavalent chromium (Cr(VI)) is an essential component in many industrial applications, including electroplating, leather tanning, and anti-corrosion steel, despite its carcinogenicity and mutagenicity (Shi et al., 1994; Salnikow and Zhitkovich, 2008). Compared to other oxidation states of Cr ions, Cr(III) is relatively benign with significantly lower toxicity since it can be excreted from the human body. Hence, photocatalytic reduction of Cr(IV) to Cr(III) is considered as an effective route. Long et al. prepared BiOBr-Bi_2S_3 heterojunctions *via* ion-exchange (Long et al., 2021). The performance of photo-reduced Cr(VI) was about 28.9 and 184.6 times higher than those of pure Bi_2S_3 and BiOBr, respectively. More importantly, the novel composite had a good Cr(III) adsorption efficiency, suggesting that it can be a bifunctional photocatalyst. Similar Cr (VI) removal was also finished with $CoFe_2O_4$/BiOBr/graphene, (Li et al., 2019), BiOCl/Bi_2S_3 (Lu et al., 2020), and $BiOCl_xBr_{1-x}$ (Hussain et al., 2020). However, there is no example of using BiOX as photocatalysts into the reduction of other heavy metal ions.

Photocatalyst Recovery

Although numerous modified BiOX had been developed and used on photocatalytic degradation, they still faced limitation during the practical application. One of the major challenges that the photocatalysts confront is the inefficient separation and recovery from the aqueous medium after being utilized in the wastewater treatment process. An *et al.* collected the Cu-doped BiOBr from suspension by centrifuge and then regenerated it by heating at 200°C to remove the residual organic (Lv et al., 2020). Although this method is effective for the recovery of photocatalysts, the process is time consuming and that inevitably raises the treatment cost. The immobilization of photocatalysts on a certain supporting substrate provides a dual advantage; the first is the efficient separation and easy recovery of reused photocatalysts, and the second is the prevention of agglomeration of the photocatalysts for higher photocatalytic performance (Tettey et al., 2010; Cao C. Y. et al., 2012). A wide range of substrates have been employed for the immobilization of BiOX, such as activated carbon, ceramic fibers, and ceramic paper (Yadav et al., 2019; Kása et al., 2020; Yadav et al., 2020). The novel green BiOX (Cl, Br and I) was homogeneously immobilized on Al_2O_3-based ceramic fiber sheets, which exhibited an excellent photocatalytic performance and recyclability for MO, bisphenol A, and ampicillin disintegration under visible-light irradiation (Yadav et al., 2019).

SUMMARY AND PROSPECTS

BiOX-based materials are prospective photocatalysts for environmental treatments, such as waste water remediation, organic pollutant degradation, and heavy metal removal. Therefore, the literature on BiOX (X = Cl, Br, I) was reviewed and discussed to provide some guidance for future studies.

Until now, heat treatments including solvothermal and hydrothermal methods are the most widely used to prepare

BiOX. These routes allow researchers to control the morphology, specific surface area, dimension, and pore size and volume. However, this is a time- and energy-consuming process. Therefore, future studies shall focus on a facile method for large-scale synthesis of more attractive BiOBr photocatalysts. The microwave-assisted method allows for the rapid production of BiOX, but the research of this process is still in its infancy.

To boost the activity of BiOX-based semiconductor photocatalysts, researchers are using diverse solutions, such as heterojunction engineering, ion doping, interfacing with carbon materials, coupling with noble metals, and facet control. Although much effort has been dedicated to regulating BiOX-based materials and optimizing their photocatalytic performance, the research in this area is still faced with a lot of challenges, and it is also filled with opportunities. In view of 2D materials, the reduction of atomic layer thickness may bring new properties that the bulk materials do not possess. The layered structure of BiOX enables it to readily form a single layer or few-layer structure. Therefore, researchers may pay attention to control preparation of BiOX with atomic thickness and explore their photocatalytic performance. The defect engineering has been verified to regulate the photocatalytic activity of BiOX, but most of the defect type in BiOX is still oxygen vacancy. More defects have not been constructed in BiOX including halogen vacancies and dual vacancies, which will interact with surface adsorbates during photocatalysis. Furthermore, in the presence of these defects, new electronic states may be induced and affect the electron transfer. Therefore, the investigation of the relationship between defect types and photocatalytic activity is a promising work in the future.

Apart from the modification of BiOX, the exploration of catalytic mechanisms at the atomic level during multiple photocatalytic applications is much needed. The catalytic sites are crucially important and thus it should be determined through calculation or direct experimental observation. More *in situ* characterization should be performed to gain atomic-level insight into the relationship between active sites and photocatalytic activity, which will guide the design direction of BiOX.

Last, photocatalytic oxidation of organic molecules was reviewed, but most of the works focused on the organic dye degradation at the laboratory scale. However, for practical application of BiOX, the treatment of organics in real water/wastewater is still a challenge, which is mainly due to the existence of dissolved inorganic ions. The photoreduction of heavy metals over BiOX is another important field that shall be investigated in the future. Taking the practical application into consideration, the immobilization techniques for the recovery of material is also important for the development.

AUTHOR CONTRIBUTIONS

XL prepared and wrote the article, and FL and XH further edited the manuscript and checked the English writing.

REFERENCES

Ai, L., Zeng, Y., and Jiang, J. (2014). Hierarchical Porous BiOI Architectures: Facile Microwave Nonaqueous Synthesis, Characterization and Application in the Removal of Congo Red from Aqueous Solution. *Chem. Eng. J.* 235, 331–339. doi:10.1016/j.cej.2013.09.046

Alansi, A. M., Qahtan, T. F., and Saleh, T. A. (2021). Solar-Driven Fixation of Bismuth Oxyhalides on Reduced Graphene Oxide for Efficient Sunlight-Responsive Immobilized Photocatalytic Systems. *Adv. Mater. Inter.* 8, 2001463. doi:10.1002/admi.202001463

Armelao, L., Bottaro, G., Maccato, C., and Tondello, E. (2012). Bismuth Oxychloride Nanoflakes: Interplay between Composition-Structure and Optical Properties. *Dalton Trans.* 41, 5480–5485. doi:10.1039/c2dt12098d

Bárdos, E., Király, A. K., Pap, Z., Baia, L., Garg, S., and Hernádi, K. (2019). The Effect of the Synthesis Temperature and Duration on the Morphology and Photocatalytic Activity of BiOX (X= Cl, Br, I) Materials. *Appl. Surf. Sci.* 479, 745–756. doi:10.1016/j.apsusc.2019.02.136

Bárdos, E., Márta, V., Baia, L., Todea, M., Kovács, G., Baán, K., et al. (2020). Hydrothermal Crystallization of Bismuth Oxybromide (BiOBr) in the Presence of Different Shape Controlling Agents. *Appl. Surf. Sci.* 518, 146184. doi:10.1016/j.apsusc.2020.146184

Bi, C., Cao, J., Lina, H., Wang, Y., and Chen, S. (2016). Enhanced Photocatalytic Activity of Bi12O17Cl2 through Loading Pt Quantum Dots as a Highly Efficient Electron Capturer. *Appl. Catal. B: Environ.* 195, 132–140. doi:10.1016/j.apcatb.2016.05.011

Bi, J., Wu, L., Li, J., Li, Z., Wang, X., and Fu, X. (2007). Simple Solvothermal Routes to Synthesize Nanocrystalline Bi2MoO6 Photocatalysts with Different Morphologies. *Acta Materialia* 55, 4699–4705. doi:10.1016/j.actamat.2007.04.034

Brain, R. A., Johnson, D. J., Richards, S. M., Sanderson, H., Sibley, P. K., and Solomon, K. R. (2004). Effects of 25 Pharmaceutical Compounds to Lemna Gibba Using a Seven-Day Static-Renewal Test. *Environ. Toxicol. Chem.* 23, 371–382. doi:10.1897/02-576

Brown, M. A., and De Vito, S. C. (1993). Predicting Azo Dye Toxicity. *Crit. Rev. Environ. Sci. Techn.* 23, 249–324. doi:10.1080/10643389309388453

Bueno, M. J. M., Gomez, M. J., Herrera, S., Hernando, M. D., Agüera, A., and Fernández-Alba, A. R. (2012). Occurrence and Persistence of Organic Emerging Contaminants and Priority Pollutants in Five Sewage Treatment Plants of Spain: Two Years Pilot Survey Monitoring. *Environ. Pollut.* 164, 267–273. doi:10.1016/j.envpol.2012.01.038

Cao, C.-Y., Qu, J., Wei, F., Liu, H., and Song, W.-G. (2012). Superb Adsorption Capacity and Mechanism of Flowerlike Magnesium Oxide Nanostructures for lead and Cadmium Ions. *ACS Appl. Mater. Inter.* 4, 4283–4287. doi:10.1021/am300972z

Cao, C., Xiao, L., Chen, C., and Cao, Q. (2015). Synthesis of Novel Cu2O/BiOCl Heterojunction Nanocomposites and Their Enhanced Photocatalytic Activity under Visible Light. *Appl. Surf. Sci.* 357, 1171–1179. doi:10.1016/j.apsusc.2015.09.121

Cao, F., Wang, Y., Wang, J., Lv, X., Liu, D., Ren, J., et al. (2018). Oxygen Vacancy Induced superior Visible-Light-Driven Photodegradation Pollutant Performance in BiOCl Microflowers. *New J. Chem.* 42, 3614–3618. doi:10.1039/c7nj04041e

Cao, J., Li, X., Lin, H., Chen, S., and Fu, X. (2012). *In Situ* preparation of Novel P-N junction Photocatalyst BiOI/(BiO)2CO3 with Enhanced Visible Light Photocatalytic Activity. *J. Hazard. Mater.* 239-240, 316–324. doi:10.1016/j.jhazmat.2012.08.078

Carlsen, L., Bruggemann, R., and Sailaukhanuly, Y. (2013). Application of Selected Partial Order Tools to Analyze Fate and Toxicity Indicators of Environmentally Hazardous Chemicals. *Ecol. Indicators* 29, 191–202. doi:10.1016/j.ecolind.2012.12.028

Chai, B., Yan, J., Fan, G., Song, G., and Wang, C. (2019). *In-situ* Construction of Bi2SiO5/BiOBr Heterojunction with Significantly Improved Photocatalytic

Activity under Visible Light. *J. Alloys Compd.* 802, 301–309. doi:10.1016/j.jallcom.2019.06.195

Chang, A.-M., Chen, Y.-H., Lai, C.-C., and Pu, Y.-C. (2021). Synergistic Effects of Surface Passivation and Charge Separation to Improve Photo-Electrochemical Performance of BiOI Nanoflakes by Au Nanoparticle Decoration. *ACS Appl. Mater. Inter.* 13, 5721–5730. doi:10.1021/acsami.0c18430

Chang, L., Pu, Y., Shen, G., Cui, Y., Wei, X., Cao, B., et al. (2020). Excellent Adsorption-Photocatalysis Synergistic Activity of 3D-3D Flower-like BiOBr/graphene Hydrogel Composite and the Removal of Potassium Butyl Xanthate. *New J. Chem.* 44, 2479–2488. doi:10.1039/c9nj06060j

Chang, X., Huang, J., Cheng, C., Sui, Q., Sha, W., Ji, G., et al. (2010). BiOX (X = Cl, Br, I) Photocatalysts Prepared Using NaBiO3 as the Bi Source: Characterization and Catalytic Performance. *Catal. Commun.* 11, 460–464. doi:10.1016/j.catcom.2009.11.023

Chen, L., Huang, R., Xiong, M., Yuan, Q., He, J., Jia, J., et al. (2013). Room-Temperature Synthesis of Flower-like BiOX (X═Cl, Br, I) Hierarchical Structures and Their Visible-Light Photocatalytic Activity. *Inorg. Chem.* 52, 11118–11125. doi:10.1021/ic401349j

Chen, M., and Chu, W. (2015). Photocatalytic Degradation and Decomposition Mechanism of Fluoroquinolones Norfloxacin over Bismuth Tungstate: experiment and Mathematic Model. *Appl. Catal. B: Environ.* 168-169, 175–182. doi:10.1016/j.apcatb.2014.12.023

Chen, S., Zhang, J., Zhang, C., Yue, Q., Li, Y., and Li, C. (2010). Equilibrium and Kinetic Studies of Methyl orange and Methyl Violet Adsorption on Activated Carbon Derived from Phragmites Australis. *Desalination* 252, 149–156. doi:10.1016/j.desal.2009.10.010

Chen, X., Liu, L., and Huang, F. (2015). Black Titanium Dioxide (TiO2) Nanomaterials. *Chem. Soc. Rev.* 44, 1861–1885. doi:10.1039/c4cs00330f

Chen, Z. G., Zhu, L., Xia, J. X., Xu, L., Li, H. M., Zhang, J., et al. (2014). Synthesis of Flower-like Pd/BiOCl Composites via Reactable Ionic Liquid and Their Enhanced Photocatalytic Properties. *Mater. Techn.* 29, 245–251. doi:10.1179/1753555714y.0000000146

Chen, Z., Liao, J., Chen, Y., Zhang, J., Fan, W., and Huang, Y. (2016). Synthesis of Oxygen Deficient BiOI for Photocatalytic Degradation of Methyl orange. *Inorg. Chem. Commun.* 74, 39–41. doi:10.1016/j.inoche.2016.10.035

Chen, Z., Zeng, J., Di, J., Zhao, D., Ji, M., Xia, J., et al. (2017). Facile Microwave-Assisted Ionic Liquid Synthesis of Sphere-like BiOBr Hollow and Porous Nanostructures with Enhanced Photocatalytic Performance. *Green. Energ. Environ.* 2, 124–133. doi:10.1016/j.gee.2017.01.005

Cheng, H., Huang, B., and Dai, Y. (2014). Engineering BiOX (X = Cl, Br, I) Nanostructures for Highly Efficient Photocatalytic Applications. *Nanoscale* 6, 2009–2026. doi:10.1039/c3nr05529a

Cheng, H., Huang, Y., Wu, J., Ling, Y., Dong, L., Zha, J., et al. (2020). Controllable Design of Bismuth Oxyiodides by *In-Situ* Self-Template Phase Transformation and Heterostructure Construction for Photocatalytic Removal of Gas-phase Mercury. *Mater. Res. Bull.* 131, 110968. doi:10.1016/j.materresbull.2020.110968

Choi, Y. I., Jeon, K. H., Kim, H. S., Lee, J. H., Park, S. J., Roh, J. E., et al. (2016). TiO2/BiOX (X=Cl, Br, I) Hybrid Microspheres for Artificial Waste Water and Real Sample Treatment under Visible Light Irradiation. *Separat. Purif. Techn.* 160, 28–42. doi:10.1016/j.seppur.2016.01.009

Chou, S.-Y., Chung, W.-H., Chen, L.-W., Dai, Y.-M., Lin, W.-Y., Lin, J.-H., et al. (2016). A Series of BiOxIy/GO Photocatalysts: Synthesis, Characterization, Activity, and Mechanism. *RSC Adv.* 6, 82743–82758. doi:10.1039/c6ra12482h

Cui, D., Wang, L., Xu, K., Ren, L., Wang, L., Yu, Y., et al. (2018). Band-gap Engineering of BiOCl with Oxygen Vacancies for Efficient Photooxidation Properties under Visible-Light Irradiation. *J. Mater. Chem. A.* 6, 2193–2199. doi:10.1039/c7ta09897a

Cui, P., Wang, J., Wang, Z., Chen, J., Xing, X., Wang, L., et al. (2016). Bismuth Oxychloride Hollow Microspheres with High Visible Light Photocatalytic Activity. *Nano Res.* 9, 593–601. doi:10.1007/s12274-015-0939-z

Dai, W.-W., and Zhao, Z.-Y. (2017). Understanding the Interfacial Properties of Graphene-Based materials/BiOI Heterostructures by DFT Calculations. *Appl. Surf. Sci.* 406, 8–20. doi:10.1016/j.apsusc.2017.02.079

Daneshvar, N., Salari, D., and Khataee, A. R. (2004). Photocatalytic Degradation of Azo Dye Acid Red 14 in Water on ZnO as an Alternative Catalyst to TiO2. *J. Photochem. Photobiol. A: Chem.* 162, 317–322. doi:10.1016/s1010-6030(03)00378-2

Derikvand, L., and Tahmasebi, N. (2021). Synthesis and Photocatalytic Performance of Bi2WO6/BiOX (X=Cl, Br, I) Composites for RhB Degradation under Visible Light. *Korean J. Chem. Eng.* 38, 163–169. doi:10.1007/s11814-020-0687-y

Di, J., Chen, C., Zhu, C., Long, R., Chen, H., Cao, X., et al. (2021). Surface Local Polarization Induced by Bismuth-Oxygen Vacancy Pairs Tuning Non-Covalent Interaction for CO 2 Photoreduction. *Adv. Energ. Mater.* 11, 2102389. doi:10.1002/aenm.202102389

Di, J., Song, P., Zhu, C., Chen, C., Xiong, J., Duan, M., et al. (2020). Strain-Engineering of Bi12O17Br2 Nanotubes for Boosting Photocatalytic CO2 Reduction. *ACS Mater. Lett.* 2, 1025–1032. doi:10.1021/acsmaterialslett.0c00306

Di, J., Xia, J., Chisholm, M. F., Zhong, J., Chen, C., Cao, X., et al. (2019). Defect-Tailoring Mediated Electron-Hole Separation in Single-Unit-Cell Bi 3 O 4 Br Nanosheets for Boosting Photocatalytic Hydrogen Evolution and Nitrogen Fixation. *Adv. Mater.* 31, 1807576. doi:10.1002/adma.201807576

Di, J., Xia, J., Ge, Y., Xu, L., Xu, H., He, M., et al. (2014). Reactable Ionic Liquid-Assisted Rapid Synthesis of BiOI Hollow Microspheres at Room Temperature with Enhanced Photocatalytic Activity. *J. Mater. Chem. A.* 2, 15864–15874. doi:10.1039/c4ta02400a

Di, J., Xia, J., Ji, M., Wang, B., Li, X., Zhang, Q., et al. (2016). Nitrogen-doped Carbon Quantum dots/BiOBr Ultrathin Nanosheets: *In Situ* strong Coupling and Improved Molecular Oxygen Activation Ability under Visible Light Irradiation. *ACS Sustain. Chem. Eng.* 4, 136–146. doi:10.1021/acssuschemeng.5b00862

Di, J., Xia, J., Ji, M., Wang, B., Yin, S., Zhang, Q., et al. (2015). Carbon Quantum Dots Modified BiOCl Ultrathin Nanosheets with Enhanced Molecular Oxygen Activation Ability for Broad Spectrum Photocatalytic Properties and Mechanism Insight. *ACS Appl. Mater. Inter.* 7, 20111–20123. doi:10.1021/acsami.5b05268

Di, J., Xia, J., Li, H., Guo, S., and Dai, S. (2017). Bismuth Oxyhalide Layered Materials for Energy and Environmental Applications. *Nano Energy* 41, 172–192. doi:10.1016/j.nanoen.2017.09.008

Di, J., Xiong, J., Li, H., and Liu, Z. (2018a). Ultrathin 2D Photocatalysts: Electronic-Structure Tailoring, Hybridization, and Applications. *Adv. Mater.* 30, 1704548. doi:10.1002/adma.201704548

Di, J., Yan, C., Handoko, A. D., Seh, Z. W., Li, H., and Liu, Z. (2018b). Ultrathin Two-Dimensional Materials for Photo- and Electrocatalytic Hydrogen Evolution. *Mater. Today* 21, 749–770. doi:10.1016/j.mattod.2018.01.034

Ding, L., Wei, R., Chen, H., Hu, J., and Li, J. (2015). Controllable Synthesis of Highly Active BiOCl Hierarchical Microsphere Self-Assembled by Nanosheets with Tunable Thickness. *Appl. Catal. B: Environ.* 172-173, 91–99. doi:10.1016/j.apcatb.2015.02.019

Fatta-Kassinos, D., Meric, S., and Nikolaou, A. (2011). Pharmaceutical Residues in Environmental Waters and Wastewater: Current State of Knowledge and Future Research. *Anal. Bioanal. Chem.* 399, 251–275. doi:10.1007/s00216-010-4300-9

Fu, H., Pan, C., Yao, W., and Zhu, Y. (2005). Visible-Light-Induced Degradation of Rhodamine B by Nanosized Bi2WO6. *J. Phys. Chem. B* 109, 22432–22439. doi:10.1021/jp052995j

Gadhi, T. A., Hernández-Gordillo, A., Bizarro, M., Jagdale, P., Tagliaferro, A., and Rodil, S. E. (2016). Efficient α/β-Bi 2 O 3 Composite for the Sequential Photodegradation of Two-Dyes Mixture. *Ceramics Int.* 42, 13065–13073. doi:10.1016/j.ceramint.2016.05.087

Ganose, A. M., Cuff, M., Butler, K. T., Walsh, A., and Scanlon, D. O. (2016). Interplay of Orbital and Relativistic Effects in Bismuth Oxyhalides: BiOF, BiOCl, BiOBr, and BiOI. *Chem. Mater.* 28, 1980–1984. doi:10.1021/acs.chemmater.6b00349

Gao, P., Yang, Y., Yin, Z., Kang, F., Fan, W., Sheng, J., et al. (2021). A Critical Review on Bismuth Oxyhalide Based Photocatalysis for Pharmaceutical Active Compounds Degradation: Modifications, Reactive Sites, and Challenges. *J. Hazard. Mater.* 412, 125186. doi:10.1016/j.jhazmat.2021.125186

Gao, Y., Wang, L., Li, Z., Li, C., Cao, X., Zhou, A., et al. (2014). Microwave-assisted Synthesis of Flower-like Ag-BiOCl Nanocomposite with Enhanced Visible-Light Photocatalytic Activity. *Mater. Lett.* 136, 295–297. doi:10.1016/j.matlet.2014.08.026

Garg, S., Yadav, M., Chandra, A., Gahlawat, S., Ingole, P. P., Pap, Z., et al. (2018b). Plant Leaf Extracts as Photocatalytic Activity Tailoring Agents for BiOCl

towards Environmental Remediation. *Ecotoxicology Environ. Saf.* 165, 357–366. doi:10.1016/j.ecoenv.2018.09.024

Garg, S., Yadav, M., Chandra, A., and Hernadi, K. (2019). A Review on BiOX (X= Cl, Br and I) Nano-/microstructures for Their Photocatalytic Applications. *J. Nanosci. Nanotechnol.* 19, 280–294. doi:10.1166/jnn.2019.15771

Garg, S., Yadav, M., Chandra, A., Sapra, S., Gahlawat, S., Ingole, P., et al. (2018a). Facile green Synthesis of BiOBr Nanostructures with superior Visible-Light-Driven Photocatalytic Activity. *Materials* 11, 1273. doi:10.3390/ma11081273

Grzechulska, J., and Morawski, A. W. (2002). Photocatalytic Decomposition of Azo-Dye Acid Black 1 in Water over Modified Titanium Dioxide. *Appl. Catal. B: Environ.* 36, 45–51. doi:10.1016/s0926-3373(01)00275-2

Guo, C., Gao, S., Lv, J., Hou, S., Zhang, Y., and Xu, J. (2017). Assessing the Photocatalytic Transformation of Norfloxacin by BiOBr/iron Oxides Hybrid Photocatalyst: Kinetics, Intermediates, and Influencing Factors. *Appl. Catal. B: Environ.* 205, 68–77. doi:10.1016/j.apcatb.2016.12.032

Guo, J., Li, X., Liang, J., Yuan, X., Jiang, L., Yu, H., et al. (2021). Fabrication and Regulation of Vacancy-Mediated Bismuth Oxyhalide towards Photocatalytic Application: Development Status and Tendency. *Coord. Chem. Rev.* 443, 214033. doi:10.1016/j.ccr.2021.214033

Han, L., Guo, Y., Lin, Z., and Huang, H. (2020). 0D to 3D Controllable Nanostructures of BiOBr via a Facile and Fast Room-Temperature Strategy. *Colloids Surf. A: Physicochemical Eng. Aspects* 603, 125233. doi:10.1016/j.colsurfa.2020.125233

Hao, R., Xiao, X., Zuo, X., Nan, J., and Zhang, W. (2012). Efficient Adsorption and Visible-Light Photocatalytic Degradation of Tetracycline Hydrochloride Using Mesoporous BiOI Microspheres. *J. Hazard. Mater.* 209-210, 137–145. doi:10.1016/j.jhazmat.2012.01.006

He, J., Wang, J., Liu, Y., Mirza, Z. A., Zhao, C., and Xiao, W. (2015). Microwave-assisted Synthesis of BiOCl and its Adsorption and Photocatalytic Activity. *Ceramics Int.* 41, 8028–8033. doi:10.1016/j.ceramint.2015.02.152

Heidari, S., Haghighi, M., and Shabani, M. (2020). Sunlight-activated BiOCl/BiOBr-Bi24O31Br10 Photocatalyst for the Removal of Pharmaceutical Compounds. *J. Clean. Prod.* 259, 120679. doi:10.1016/j.jclepro.2020.120679

Henle, J., Simon, P., Frenzel, A., Scholz, S., and Kaskel, S. (2007). Nanosized BiOX (X = Cl, Br, I) Particles Synthesized in Reverse Microemulsions. *Chem. Mater.* 19, 366–373. doi:10.1021/cm061671k

Herrmann, J.-M. (1999). Heterogeneous Photocatalysis: Fundamentals and Applications to the Removal of Various Types of Aqueous Pollutants. *Catal. Today* 53, 115–129. doi:10.1016/s0920-5861(99)00107-8

Herrmann, J.-M. (2005). Heterogeneous Photocatalysis: State of the Art and Present Applications in Honor of Pr. R.L. Burwell Jr. (1912-2003), Former Head of Ipatieff Laboratories, Northwestern University, Evanston (Ill). *Top. Catal.* 34, 49–65. doi:10.1007/s11244-005-3788-2

Hidalgo, M. C., Aguilar, M., Maicu, M., Navío, J. A., and Colón, G. (2007). Hydrothermal Preparation of Highly Photoactive TiO2 Nanoparticles. *Catal. Today* 129, 50–58. doi:10.1016/j.cattod.2007.06.053

Hoffmann, M. R., Martin, S. T., Choi, W., and Bahnemann, D. W. (1995). Environmental Applications of Semiconductor Photocatalysis. *Chem. Rev.* 95, 69–96. doi:10.1021/cr00033a004

Huang, H., Xiao, K., Zhang, T., Dong, F., and Zhang, Y. (2017). Rational Design on 3D Hierarchical Bismuth Oxyiodides via *In Situ* Self-Template Phase Transformation and Phase-junction Construction for Optimizing Photocatalysis against Diverse Contaminants. *Appl. Catal. B: Environ.* 203, 879–888. doi:10.1016/j.apcatb.2016.10.082

Huang, W. L., and Zhu, Q. (2008). Electronic Structures of Relaxed BiOX (X=F, Cl, Br, I) Photocatalysts. *Comput. Mater. Sci.* 43, 1101–1108. doi:10.1016/j.commatsci.2008.03.005

Huang, Y., Li, H., Balogun, M.-S., Liu, W., Tong, Y., Lu, X., et al. (2014). Oxygen Vacancy Induced Bismuth Oxyiodide with Remarkably Increased Visible-Light Absorption and superior Photocatalytic Performance. *ACS Appl. Mater. Inter.* 6, 22920–22927. doi:10.1021/am507641k

Huizhong, A., Yi, D., Tianmin, W., Cong, W., Weichang, H., and Zhang, J. (2008). Photocatalytic Properties of Biox (X= Cl, Br, and I). *Rare Met.* 27, 243–250. doi:10.1016/S1001-0521(08)60123-0

Hussain, M. B., Khan, M. S., Loussala, H. M., and Bashir, M. S. (2020). The Synthesis of a BiOClxBr1−x Nanostructure Photocatalyst with High Surface Area for the Enhanced Visible-Light Photocatalytic Reduction of Cr(vi). *RSC Adv.* 10, 4763–4771. doi:10.1039/c9ra10256f

Jalalah, M., Faisal, M., Bouzid, H., Park, J.-G., Al-Sayari, S. A., and Ismail, A. A. (2015). Comparative Study on Photocatalytic Performances of Crystalline α- and β-Bi2O3 Nanoparticles under Visible Light. *J. Ind. Eng. Chem.* 30, 183–189. doi:10.1016/j.jiec.2015.05.020

Jia, M., Hu, X., Wang, S., Huang, Y., and Song, L. (2015). Photocatalytic Properties of Hierarchical BiOXs Obtained via an Ethanol-Assisted Solvothermal Process. *J. Environ. Sci.* 35, 172–180. doi:10.1016/j.jes.2014.09.045

Jia, T., Wu, J., Song, J., Liu, Q., Wang, J., Qi, Y., et al. (2020a). *In Situ* self-growing 3D Hierarchical BiOBr/BiOIO3 Z-Scheme Heterojunction with Rich Oxygen Vacancies and Iodine Ions as Carriers Transfer Dual-Channels for Enhanced Photocatalytic Activity. *Chem. Eng. J.* 396, 125258. doi:10.1016/j.cej.2020.125258

Jia, T., Yang, J., Zhang, Y., Ji, L., Chen, Y., Wang, D., et al. (2020b). Facet-dependent Flower-like BiOBr with Exposed the (0 0 1) and (0 1 0) Facets for Enhanced Charge Carrier Transfer and Photocatalytic Oxidation Activity. *Chem. Phys. Lett.* 760, 138010. doi:10.1016/j.cplett.2020.138010

Jiang, D., and Li, X. (2015). Advanced Photocatalysts with Nanoheterostructures. *Mater. Focus* 4, 14–19. doi:10.1166/mat.2015.1216

Jiang, G., Wang, R., Wang, X., Xi, X., Hu, R., Zhou, Y., et al. (2012). Novel Highly Active Visible-Light-Induced Photocatalysts Based on BiOBr with Ti Doping and Ag Decorating. *ACS Appl. Mater. Inter.* 4, 4440–4444. doi:10.1021/am301177k

Jiang, J., Zhao, K., Xiao, X., and Zhang, L. (2012). Synthesis and Facet-dependent Photoreactivity of BiOCl Single-Crystalline Nanosheets. *J. Am. Chem. Soc.* 134, 4473–4476. doi:10.1021/ja210484t

Jiang, L., Zhou, G., Mi, J., and Wu, Z. (2012). Fabrication of Visible-Light-Driven One-Dimensional Anatase TiO2/Ag Heterojunction Plasmonic Photocatalyst. *Catal. Commun.* 24, 48–51. doi:10.1016/j.catcom.2012.03.017

Jiang, R., Lu, G., Yan, Z., Wu, D., Zhou, R., and Bao, X. (2019). Insights into a CQD-SnNb2O6/BiOCl Z-Scheme System for the Degradation of Benzocaine: Influence Factors, Intermediate Toxicity and Photocatalytic Mechanism. *Chem. Eng. J.* 374, 79–90. doi:10.1016/j.cej.2019.05.176

Jiang, T., Li, J., Gao, Y., Li, L., Lu, T., and Pan, L. (2017). BiOBr/BiOF Composites for Efficient Degradation of Rhodamine B and Nitrobenzene under Visible Light Irradiation. *J. Colloid Interf. Sci.* 490, 812–818. doi:10.1016/j.jcis.2016.12.007

Jin, X., Lv, C., Zhou, X., Zhang, C., Zhang, B., Su, H., et al. (2018). Realizing the Regulated Carrier Separation and Exciton Generation of Bi24O31Cl10via a Carbon Doping Strategy. *J. Mater. Chem. A.* 6, 24350–24357. doi:10.1039/c8ta08598f

Juntrapirom, S., Tantraviwat, D., Suntalelat, S., Thongsook, O., Phanichphant, S., and Inceesungvorn, B. (2017). Visible Light Photocatalytic Performance and Mechanism of Highly Efficient SnS/BiOI Heterojunction. *J. Colloid Interf. Sci.* 504, 711–720. doi:10.1016/j.jcis.2017.06.019

Kása, Z., Orbán, E., Pap, Z., Ábrahám, I., Magyari, K., Garg, S., et al. (2020). Innovative and Cost-Efficient BiOI Immobilization Technique on Ceramic Paper-Total Coverage and High Photocatalytic Activity. *Nanomaterials* 10, 1959.

Kong, X. Y., Lee, W. P. C., Ong, W.-J., Chai, S.-P., and Mohamed, A. R. (2016). Oxygen-Deficient BiOBr as a Highly Stable Photocatalyst for Efficient CO2Reduction into Renewable Carbon-Neutral Fuels. *ChemCatChem* 8, 3074–3081. doi:10.1002/cctc.201600782

Landge, V. K., Sonawane, S. H., Sivakumar, M., Sonawane, S. S., Uday Bhaskar Babu, G., and Boczkaj, G. (2021). S-scheme Heterojunction Bi2O3-ZnO/Bentonite clay Composite with Enhanced Photocatalytic Performance. *Sustainable Energ. Tech. Assessments* 45, 101194. doi:10.1016/j.seta.2021.101194

Ledakowicz, S., and Gonera, M. (1999). Optimisation of Oxidants Dose for Combined Chemical and Biological Treatment of Textile Wastewater. *Water Res.* 33, 2511–2516. doi:10.1016/s0043-1354(98)00494-1

Lee, S.-Y., and Park, S.-J. (2013). TiO2 Photocatalyst for Water Treatment Applications. *J. Ind. Eng. Chem.* 19, 1761–1769. doi:10.1016/j.jiec.2013.07.012

Lee, Y.-H., Dai, Y.-M., Fu, J.-Y., and Chen, C.-C. (2017). A Series of Bismuth-Oxychloride/bismuth-Oxyiodide/graphene-Oxide Nanocomposites: Synthesis, Characterization, and Photcatalytic Activity and Mechanism. *Mol. Catal.* 432, 196–209. doi:10.1016/j.mcat.2017.01.002

Li, G., Qin, F., Yang, H., Lu, Z., Sun, H., and Chen, R. (2012). Facile Microwave Synthesis of 3D Flowerlike BiOBr Nanostructures and Their Excellent Cr VI

Removal Capacity. *Eur. J. Inorg. Chem.* 2012, 2508–2513. doi:10.1002/ejic.201101427

Li, H., Jia, Q., Cui, Y., and Fan, S. (2013). Photocatalytic Properties of BiOI Synthesized by a Simple Hydrothermal Process. *Mater. Lett.* 107, 262–264. doi:10.1016/j.matlet.2013.06.019

Li, H., Li, J., Ai, Z., Jia, F., and Zhang, L. (2018). Oxygen Vacancy-Mediated Photocatalysis of BiOCl: Reactivity, Selectivity, and Perspectives. *Angew. Chem. Int. Ed.* 57, 122–138. doi:10.1002/anie.201705628

Li, H., Shang, J., Ai, Z., and Zhang, L. (2015). Efficient Visible Light Nitrogen Fixation with BiOBr Nanosheets of Oxygen Vacancies on the Exposed {001} Facets. *J. Am. Chem. Soc.* 137, 6393–6399. doi:10.1021/jacs.5b03105

Li, J., Zhang, L., Li, Y., and Yu, Y. (2013). Synthesis and Internal Electric Field Dependent Photoreactivity of Bi3O4Cl Single-Crystalline Nanosheets with High {001} Facet Exposure Percentages. *Nanoscale* 6, 167–171. doi:10.1039/c3nr05246j

Li, J., Li, H., Zhan, G., and Zhang, L. (2017). Solar Water Splitting and Nitrogen Fixation with Layered Bismuth Oxyhalides. *Acc. Chem. Res.* 50, 112–121. doi:10.1021/acs.accounts.6b00523

Li, J., Zhao, K., Yu, Y., and Zhang, L. (2015). Facet-Level Mechanistic Insights into General Homogeneous Carbon Doping for Enhanced Solar-To-Hydrogen Conversion. *Adv. Funct. Mater.* 25, 2189–2201. doi:10.1002/adfm.201404178

Li, K.-L., Lee, W. W., Lu, C.-S., Dai, Y.-M., Chou, S.-Y., Chen, H.-L., et al. (2014). Synthesis of BiOBr, Bi3O4Br, and Bi12O17Br2 by Controlled Hydrothermal Method and Their Photocatalytic Properties. *J. Taiwan Inst. Chem. Eng.* 45, 2688–2697. doi:10.1016/j.jtice.2014.04.001

Li, L., Salvador, P. A., and Rohrer, G. S. (2014). Photocatalysts with Internal Electric fields. *Nanoscale* 6, 24–42. doi:10.1039/c3nr03998f

Li, M., Song, C., Wu, Y., Wang, M., Pan, Z., Sun, Y., et al. (2019). Novel Z-Scheme Visible-Light Photocatalyst Based on CoFe2O4/BiOBr/Graphene Composites for Organic Dye Degradation and Cr(VI) Reduction. *Appl. Surf. Sci.* 478, 744–753. doi:10.1016/j.apsusc.2019.02.017

Li, P., Cao, W., Zhu, Y., Teng, Q., Peng, L., Jiang, C., et al. (2020). NaOH-induced Formation of 3D Flower-Sphere BiOBr/Bi4O5Br2 with Proper-Oxygen Vacancies via *In-Situ* Self-Template Phase Transformation Method for Antibiotic Photodegradation. *Sci. Total Environ.* 715, 136809. doi:10.1016/j.scitotenv.2020.136809

Li, R., Gao, X., Fan, C., Zhang, X., Wang, Y., and Wang, Y. (2015). A Facile Approach for the Tunable Fabrication of BiOBr Photocatalysts with High Activity and Stability. *Appl. Surf. Sci.* 355, 1075–1082. doi:10.1016/j.apsusc.2015.07.216

Li, W. T., Huang, W. Z., Zhou, H., Yin, H. Y., Zheng, Y. F., and Song, X. C. (2015). Synthesis of Zn2+ Doped BiOCl Hierarchical Nanostructures and Their Exceptional Visible Light Photocatalytic Properties. *J. Alloys Compd.* 638, 148–154. doi:10.1016/j.jallcom.2015.03.103

Li, W., Zou, Y., Geng, X., Xiao, F., An, G., and Wang, D. (2017). Constructing Highly Catalytic Oxidation over BiOBr-Based Hierarchical Microspheres: Importance of Redox Potential of Doped Cations. *Mol. Catal.* 438, 19–29. doi:10.1016/j.mcat.2017.05.017

Li, X., Wang, T., Tao, X., Qiu, G., Li, C., and Li, B. (2020). Interfacial Synergy of Pd Sites and Defective BiOBr for Promoting the Solar-Driven Selective Oxidation of Toluene. *J. Mater. Chem. A.* 8, 17657–17669. doi:10.1039/d0ta05733a

Li, Y., Qin, H., Sun, H., Zhang, M., Wang, J., Yao, H., et al. (2015). Synthesis of BiOI Hierarchical Nanospheres and Their Application in Photocatalysis. *Mater. Lett.* 152, 248–251. doi:10.1016/j.matlet.2015.03.126

Li, Z., Qu, Y., Hu, K., Humayun, M., Chen, S., and Jing, L. (2017). Improved Photoelectrocatalytic Activities of BiOCl with High Stability for Water Oxidation and MO Degradation by Coupling RGO and Modifying Phosphate Groups to Prolong Carrier Lifetime. *Appl. Catal. B: Environ.* 203, 355–362. doi:10.1016/j.apcatb.2016.10.045

Lin, J., Shen, J., Wang, R., Cui, J., Zhou, W., Hu, P., et al. (2011). Nano-p-n Junctions on Surface-Coarsened TiO2 Nanobelts with Enhanced Photocatalytic Activity. *J. Mater. Chem.* 21, 5106–5113. doi:10.1039/c0jm04131a

Lin, W., Yu, X., Shen, Y., Chen, H., Zhu, Y., Zhang, Y., et al. (2017). Carbon dots/BiOCl Films with Enhanced Visible Light Photocatalytic Performance. *J. Nanopart. Res.* 19, 56. doi:10.1007/s11051-017-3764-3

Lin, Z.-R., Zhao, L., and Dong, Y.-H. (2015). Quantitative Characterization of Hydroxyl Radical Generation in a Goethite-Catalyzed Fenton-like Reaction. *Chemosphere* 141, 7–12. doi:10.1016/j.chemosphere.2015.05.066

Linsebigler, A. L., Lu, G., and Yates, J. T., Jr (1995). Photocatalysis on TiO2 Surfaces: Principles, Mechanisms, and Selected Results. *Chem. Rev.* 95, 735–758. doi:10.1021/cr00035a013

Liu, C., Nanaboina, V., Korshin, G. V., and Jiang, W. (2012). Spectroscopic Study of Degradation Products of Ciprofloxacin, Norfloxacin and Lomefloxacin Formed in Ozonated Wastewater. *Water Res.* 46, 5235–5246. doi:10.1016/j.watres.2012.07.005

Liu, C., Zhou, J., Su, J., and Guo, L. (2019). Turning the Unwanted Surface Bismuth Enrichment to Favourable BiVO4/BiOCl Heterojunction for Enhanced Photoelectrochemical Performance. *Appl. Catal. B: Environ.* 241, 506–513. doi:10.1016/j.apcatb.2018.09.060

Liu, H., Cao, W., Su, Y., Wang, Y., and Wang, X. (2012). Synthesis, Characterization and Photocatalytic Performance of Novel Visible-Light-Induced Ag/BiOI. *Appl. Catal. B: Environ.* 111-112, 271–279. doi:10.1016/j.apcatb.2011.10.008

Liu, J., Yuan, Q., Zhao, H., and Zou, S. (2018). Efficient Room-Temperature Selective Oxidation of Benzyl Alcohol into Benzaldehyde over Pt/BiOCl Nanocomposite. *Catal. Lett.* 148, 1093–1099. doi:10.1007/s10562-018-2337-0

Liu, Y., Hu, Z., and Yu, J. C. (2021). Photocatalytic Degradation of Ibuprofen on S-Doped BiOBr. *Chemosphere* 278, 130376. doi:10.1016/j.chemosphere.2021.130376

Liu, Y., and Wu, Q. (2017). One Novel Material with High Visible-Light Activity: Hexagonal Cu Flakelets Embedded in the Petals of BiOBr Flower-Nanospheres. *J. Nanopart. Res.* 19, 55. doi:10.1007/s11051-016-3734-1

Liu, Z., Wu, B., Xiang, D., and Zhu, Y. (2012). Effect of Solvents on Morphology and Photocatalytic Activity of BiOBr Synthesized by Solvothermal Method. *Mater. Res. Bull.* 47, 3753–3757. doi:10.1016/j.materresbull.2012.06.026

Liu, Z., Wu, B., Zhao, Y., Niu, J., and Zhu, Y. (2014). Solvothermal Synthesis and Photocatalytic Activity of Al-Doped BiOBr Microspheres. *Ceramics Int.* 40, 5597–5603. doi:10.1016/j.ceramint.2013.10.152

Long, Z., Zhang, G., Du, H., Zhu, J., and Li, J. (2021). Preparation and Application of BiOBr-Bi2S3 Heterojunctions for Efficient Photocatalytic Removal of Cr(VI). *J. Hazard. Mater.* 407, 124394. doi:10.1016/j.jhazmat.2020.124394

López-Velázquez, K., Guzmán-Mar, J. L., Montalvo-Herrera, T. J., Mendiola-Alvarez, S. Y., and Villanueva-Rodríguez, M. (2021). Efficient Photocatalytic Removal of Four Endocrine-Disrupting Compounds Using N-Doped BiOBr Catalyst under UV-Vis Radiation. *J. Environ. Chem. Eng.* 9, 106185. doi:10.1016/j.jece.2021.106185

Lu, L., Kong, L., Jiang, Z., Lai, H. H.-C., Xiao, T., and Edwards, P. P. (2012). Visible-light-driven Photodegradation of Rhodamine B on Ag-Modified BiOBr. *Catal. Lett.* 142, 771–778. doi:10.1007/s10562-012-0824-2

Lu, Y., Song, J., Li, W., Pan, Y., Fang, H., Wang, X., et al. (2020). Preparation of BiOCl/Bi2S3 Composites by Simple Ion Exchange Method for Highly Efficient Photocatalytic Reduction of Cr6+. *Appl. Surf. Sci.* 506, 145000. doi:10.1016/j.apsusc.2019.145000

Luo, W., Yang, Z., Li, Z., Zhang, J., Liu, J., Zhao, Z., et al. (2011). Solar Hydrogen Generation from Seawater with a Modified BiVO4 Photoanode. *Energy Environ. Sci.* 4, 4046–4051. doi:10.1039/c1ee01812d

Lv, X., Yan, D. Y. S., Lam, F. L.-Y., Ng, Y. H., Yin, S., and An, A. K. (2020). Solvothermal Synthesis of Copper-Doped BiOBr Microflowers with Enhanced Adsorption and Visible-Light Driven Photocatalytic Degradation of Norfloxacin. *Chem. Eng. J.* 401, 126012. doi:10.1016/j.cej.2020.126012

Lyu, J., Hu, Z., Li, Z., and Ge, M. (2019). Removal of Tetracycline by BiOBr Microspheres with Oxygen Vacancies: Combination of Adsorption and Photocatalysis. *J. Phys. Chem. Sol.* 129, 61–70. doi:10.1016/j.jpcs.2018.12.041

Ma, F.-Q., Yao, J.-W., Zhang, Y.-F., and Wei, Y. (2017). Unique Band Structure Enhanced Visible Light Photocatalytic Activity of Phosphorus-Doped BiOI Hierarchical Microspheres. *RSC Adv.* 7, 36288–36296. doi:10.1039/c7ra06261c

Ma, X., Ma, Z., Liao, T., Liu, X., Zhang, Y., Li, L., et al. (2017). Preparation of BiVO4/BiOCl Heterojunction Photocatalyst by *In-Situ* Transformation Method for Norfloxacin Photocatalytic Degradation. *J. Alloys Compd.* 702, 68–74. doi:10.1016/j.jallcom.2017.01.214

Ma, Z., Li, P., Ye, L., Zhou, Y., Su, F., Ding, C., et al. (2017). Oxygen Vacancies Induced Exciton Dissociation of Flexible BiOCl Nanosheets for Effective Photocatalytic CO2 Conversion. *J. Mater. Chem. A.* 5, 24995–25004. doi:10.1039/c7ta08766g

Maimaitizi, H., Abulizi, A., Kadeer, K., Talifu, D., and Tursun, Y. (2020). *In Situ* synthesis of Pt and N Co-doped Hollow Hierarchical BiOCl Microsphere as an

Efficient Photocatalyst for Organic Pollutant Degradation and Photocatalytic CO2 Reduction. *Appl. Surf. Sci.* 502, 144083. doi:10.1016/j.apsusc.2019.144083

Malato, S., Blanco, J., Alarcón, D. C., Maldonado, M. I., Fernández-Ibáñez, P., and Gernjak, W. (2007). Photocatalytic Decontamination and Disinfection of Water with Solar Collectors. *Catal. Today* 122, 137–149. doi:10.1016/j.cattod.2007.01.034

Malefane, M. E., Feleni, U., Mafa, P. J., and Kuvarega, A. T. (2020). Fabrication of Direct Z-Scheme Co3O4/BiOI for Ibuprofen and Trimethoprim Degradation under Visible Light Irradiation. *Appl. Surf. Sci.* 514, 145940. doi:10.1016/j.apsusc.2020.145940

Mao, D., Lü, X., Jiang, Z., Xie, J., Lu, X., Wei, W., et al. (2014). Ionic Liquid-Assisted Hydrothermal Synthesis of Square BiOBr Nanoplates with Highly Efficient Photocatalytic Activity. *Mater. Lett.* 118, 154–157. doi:10.1016/j.matlet.2013.12.049

Meng, X., and Zhang, Z. Synthesis. (2015). Analysis, and Testing of BiOBr-Bi_2WO_6 Photocatalytic Heterojunction Semiconductors. *Int. J. Photoenergy* 2015. doi:10.1155/2015/630476

Mokhtari, F., and Tahmasebi, N. (2021). Hydrothermal Synthesis of W-Doped BiOCl Nanoplates for Photocatalytic Degradation of Rhodamine B under Visible Light. *J. Phys. Chem. Sol.* 149, 109804. doi:10.1016/j.jpcs.2020.109804

Montoya-Zamora, J. M., Martínez-de la Cruz, A., and López Cuéllar, E. (2017). Enhanced Photocatalytic Activity of BiOI Synthesized in Presence of EDTA. *J. Taiwan Inst. Chem. Eng.* 75, 307–316. doi:10.1016/j.jtice.2017.03.031

Ni, Z., Sun, Y., Zhang, Y., and Dong, F. (2016). Fabrication, Modification and Application of (BiO)2CO3-based Photocatalysts: A Review. *Appl. Surf. Sci.* 365, 314–335. doi:10.1016/j.apsusc.2015.12.231

Ning, S., Ding, L., Lin, Z., Lin, Q., Zhang, H., Lin, H., et al. (2016). One-pot Fabrication of Bi3O4Cl/BiOCl Plate-On-Plate Heterojunction with Enhanced Visible-Light Photocatalytic Activity. *Appl. Catal. B: Environ.* 185, 203–212. doi:10.1016/j.apcatb.2015.12.021

Obeid, M. M., Stampfl, C., Bafekry, A., Guan, Z., Jappor, H. R., Nguyen, C. V., et al. (2020). First-principles Investigation of Nonmetal Doped Single-Layer BiOBr as a Potential Photocatalyst with a Low Recombination Rate. *Phys. Chem. Chem. Phys.* 22, 15354–15364. doi:10.1039/d0cp02007a

Oudghiri-Hassani, H., Rakass, S., Al Wadaani, F. T., Al-Ghamdi, K. J., Omer, A., Messali, M., et al. (2015). Synthesis, Characterization and Photocatalytic Activity of α-Bi2O3 Nanoparticles. *J. Taibah Univ. Sci.* 9, 508–512. doi:10.1016/j.jtusci.2015.01.009

Pan, C., and Zhu, Y. (2010). New Type of BiPO4 Oxy-Acid Salt Photocatalyst with High Photocatalytic Activity on Degradation of Dye. *Environ. Sci. Technol.* 44, 5570–5574. doi:10.1021/es101223n

Pan, C., and Zhu, Y. (2011). Size-controlled Synthesis of BiPO4 Nanocrystals for Enhanced Photocatalytic Performance. *J. Mater. Chem.* 21, 4235–4241. doi:10.1039/c0jm03655b

Pare, B., Sarwan, B., and Jonnalagadda, S. B. (2011). Photocatalytic Mineralization Study of Malachite green on the Surface of Mn-Doped BiOCl Activated by Visible Light under Ambient Condition. *Appl. Surf. Sci.* 258, 247–253. doi:10.1016/j.apsusc.2011.08.040

Park, H., Bak, A., Ahn, Y. Y., Choi, J., and Hoffmannn, M. R. (2012). Photoelectrochemical Performance of Multi-Layered BiOx-TiO2/Ti Electrodes for Degradation of Phenol and Production of Molecular Hydrogen in Water. *J. Hazard. Mater.* 211-212, 47–54. doi:10.1016/j.jhazmat.2011.05.009

Peng, Y., Xu, J., Liu, T., and Mao, Y.-g. (2017). Controlled Synthesis of One-Dimensional BiOBr with Exposed (110) Facets and Enhanced Photocatalytic Activity. *CrystEngComm* 19, 6473–6480. doi:10.1039/c7ce01452j

Peng, Y., Yan, M., Chen, Q.-G., Fan, C.-M., Zhou, H.-Y., and Xu, A.-W. (2014). Novel One-Dimensional Bi2O3-Bi2WO6 P-N Hierarchical Heterojunction with Enhanced Photocatalytic Activity. *J. Mater. Chem. A.* 2, 8517–8524. doi:10.1039/c4ta00274a

Qin, H., Wang, K., Jiang, L., Li, J., Wu, X., and Zhang, G. (2020). Ultrasonic-assisted Fabrication of a Direct Z-Scheme BiOI/Bi2O4 Heterojunction with superior Visible Light-Responsive Photocatalytic Performance. *J. Alloys Compd.* 821, 153417. doi:10.1016/j.jallcom.2019.153417

Qu, X., Alvarez, P. J. J., and Li, Q. (2013). Applications of Nanotechnology in Water and Wastewater Treatment. *Water Res.* 47, 3931–3946. doi:10.1016/j.watres.2012.09.058

Raizada, P., Priya, B., Thakur, P., and Singh, P. (2016). "Solar Light Induced Photodegradation of Oxytetracyline Using Zr Doped TiO_2/CaO Based Nanocomposite," in *Indian Journal of Chemistry* (Chennai, Tamil Nadu: Council of Scientific & Industrial Research).

Razavi-Khosroshahi, H., Mohammadzadeh, S., Hojamberdiev, M., Kitano, S., Yamauchi, M., and Fuji, M. (2019). BiVO4/BiOX (X = F, Cl, Br, I) Heterojunctions for Degrading Organic Dye under Visible Light. *Adv. Powder Techn.* 30, 1290–1296. doi:10.1016/j.apt.2019.04.002

Ren, X., Wu, K., Qin, Z., Zhao, X., and Yang, H. (2019). The Construction of Type II Heterojunction of Bi2WO6/BiOBr Photocatalyst with Improved Photocatalytic Performance. *J. Alloys Compd.* 788, 102–109. doi:10.1016/j.jallcom.2019.02.211

Richardson, S. D. (2012). Environmental Mass Spectrometry: Emerging Contaminants and Current Issues. *Anal. Chem.* 84, 747–778. doi:10.1021/ac202903d

Robinson, A. A., Belden, J. B., and Lydy, M. J. (2005). Toxicity of Fluoroquinolone Antibiotics to Aquatic Organisms. *Environ. Toxicol. Chem.* 24, 423–430. doi:10.1897/04-210r.1

Salnikow, K., and Zhitkovich, A. (2008). Genetic and Epigenetic Mechanisms in Metal Carcinogenesis and Cocarcinogenesis: Nickel, Arsenic, and Chromium. *Chem. Res. Toxicol.* 21, 28–44. doi:10.1021/tx700198a

Senasu, T., Nijpanich, S., Juabrum, S., Chanlek, N., and Nanan, S. (2021). CdS/BiOBr Heterojunction Photocatalyst with High Performance for Solar-Light-Driven Degradation of Ciprofloxacin and Norfloxacin Antibiotics. *Appl. Surf. Sci.* 567, 150850. doi:10.1016/j.apsusc.2021.150850

Shang, J., Hao, W., Lv, X., Wang, T., Wang, X., Du, Y., et al. (2014). Bismuth Oxybromide with Reasonable Photocatalytic Reduction Activity under Visible Light. *ACS Catal.* 4, 954–961. doi:10.1021/cs401025u

Sharma, K., Dutta, V., Sharma, S., Raizada, P., Hosseini-Bandegharaei, A., Thakur, P., et al. (2019). Recent Advances in Enhanced Photocatalytic Activity of Bismuth Oxyhalides for Efficient Photocatalysis of Organic Pollutants in Water: a Review. *J. Ind. Eng. Chem.* 78, 1–20. doi:10.1016/j.jiec.2019.06.022

Sharma, N., Pap, Z., Garg, S., and Hernádi, K. (2019). Hydrothermal Synthesis of BiOBr and BiOBr/CNT Composites, Their Photocatalytic Activity and the Importance of Early Bi6O6(OH)3(NO3)3·1.5H2O Formation. *Appl. Surf. Sci.* 495, 143536. doi:10.1016/j.apsusc.2019.143536

Sharma, N., Pap, Z., Kornélia, B., Gyulavari, T., Karacs, G., Nemeth, Z., et al. (2022). Effective Removal of Phenol by Activated charcoal/BiOCl Composite under UV Light Irradiation. *J. Mol. Struct.* 1254, 132344. doi:10.1016/j.molstruc.2022.132344

Sharma, N., Pap, Z., Székely, I., Focsan, M., Karacs, G., Nemeth, Z., et al. (2021). Combination of Iodine-Deficient BiOI Phases in the Presence of CNT to Enhance Photocatalytic Activity towards Phenol Decomposition under Visible Light. *Appl. Surf. Sci.* 565, 150605. doi:10.1016/j.apsusc.2021.150605

Shi, X., Mao, Y., Knapton, A. D., Ding, M., Rojanasakul, Y., Gannett, P. M., et al. (1994). Reaction of Cr(VI) with Ascorbate and Hydrogen Peroxide Generates Hydroxyl Radicals and Causes DNA Damage: Role of a Cr(IV)-mediated Fenton-like Reaction. *Carcinogenesis* 15, 2475–2478. doi:10.1093/carcin/15.11.2475

Shi, X., Wang, P., Wang, L., Bai, Y., Xie, H., Zhou, Y., et al. (2018). Few Layered BiOBr with Expanded Interlayer Spacing and Oxygen Vacancies for Efficient Decomposition of Real Oil Field Produced Wastewater. *ACS Sustain. Chem. Eng.* 6, 13739–13746. doi:10.1021/acssuschemeng.8b01622

Sin, J.-C., Lam, S.-M., Zeng, H., Lin, H., Li, H., Kugan Kumaresan, A., et al. (2020). Z-scheme Heterojunction Nanocomposite Fabricated by Decorating Magnetic MnFe2O4 Nanoparticles on BiOBr Nanosheets for Enhanced Visible Light Photocatalytic Degradation of 2,4-dichlorophenoxyacetic Acid and Rhodamine B. *Separat. Purif. Techn.* 250, 117186. doi:10.1016/j.seppur.2020.117186

Song, J., Zhang, Z., Zhi, S., Niu, B., Dong, H., Wu, D., et al. (2021). Oxygen-vacancy-rich BiOCl with 3D Network Structure for Enhanced Photocatalytic CO_2 Reduction and Antibiotic Degradation. *J. Taiwan Inst. Chem. E* 128, 380–387. doi:10.1016/j.jtice.2021.08.044

Song, Z., Dong, X., Wang, N., Zhu, L., Luo, Z., Fang, J., et al. (2017). Efficient Photocatalytic Defluorination of Perfluorooctanoic Acid over BiOCl Nanosheets via a Hole Direct Oxidation Mechanism. *Chem. Eng. J.* 317, 925–934. doi:10.1016/j.cej.2017.02.126

Sturini, M., Speltini, A., Maraschi, F., Pretali, L., Profumo, A., Fasani, E., et al. (2012). Photodegradation of Fluoroquinolones in Surface Water and

Antimicrobial Activity of the Photoproducts. *Water Res.* 46, 5575–5582. doi:10.1016/j.watres.2012.07.043

Su, J., Xiao, Y., and Ren, M. (2014). Direct Hydrolysis Synthesis of BiOI Flowerlike Hierarchical Structures and It's Photocatalytic Activity under Simulated Sunlight Irradiation. *Catal. Commun.* 45, 30–33. doi:10.1016/j.catcom.2013.10.020

Su, M., He, C., Zhu, L., Sun, Z., Shan, C., Zhang, Q., et al. (2012). Enhanced Adsorption and Photocatalytic Activity of BiOI-MWCNT Composites towards Organic Pollutants in Aqueous Solution. *J. Hazard. Mater.* 229-230, 72–82. doi:10.1016/j.jhazmat.2012.05.061

Su, X., Yang, J., Yu, X., Zhu, Y., and Zhang, Y. (2018). *In Situ* grown Hierarchical 50% BiOCl/BiOI Hollow Flowerlike Microspheres on Reduced Graphene Oxide Nanosheets for Enhanced Visible-Light Photocatalytic Degradation of Rhodamine B. *Appl. Surf. Sci.* 433, 502–512. doi:10.1016/j.apsusc.2017.09.258

Sun, Y., Qi, X., Li, R., Xie, Y., Tang, Q., and Ren, B. (2020). Hydrothermal Synthesis of 2D/2D BiOCl/g-C3n4 Z-Scheme: For TC Degradation and Antimicrobial Activity Evaluation. *Opt. Mater.* 108, 110170. doi:10.1016/j.optmat.2020.110170

Tahmasebi, N., Maleki, Z., and Farahnak, P. (2019). Enhanced Photocatalytic Activities of Bi2WO6/BiOCl Composite Synthesized by One-step Hydrothermal Method with the Assistance of HCl. *Mater. Sci. Semiconductor Process.* 89, 32–40. doi:10.1016/j.mssp.2018.08.026

Tang, X., Liu, H., Yang, C., Jin, X., Zhong, J., and Li, J. (2020). *In-situ* Fabrication of Z-Scheme CdS/BiOCl Heterojunctions with Largely Improved Photocatalytic Performance. *Colloids Surf. A: Physicochemical Eng. Aspects* 599, 124880. doi:10.1016/j.colsurfa.2020.124880

Tettey, K. E., Yee, M. Q., and Lee, D. (2010). Photocatalytic and Conductive MWCNT/TiO2 Nanocomposite Thin Films. *ACS Appl. Mater. Inter.* 2, 2646–2652. doi:10.1021/am1004656

Tian, N., Huang, H., Wang, S., Zhang, T., Du, X., and Zhang, Y. (2020). Facet-charge-induced Coupling Dependent Interfacial Photocharge Separation: A Case of BiOI/g-C3n4 P-N junction. *Appl. Catal. B: Environ.* 267, 118697. doi:10.1016/j.apcatb.2020.118697

Tollefson, J. (2011). How green Is My Future? *Nature* 473, 134–135. doi:10.1038/473134a

Tu, X., Luo, S., Chen, G., and Li, J. (2012). One-Pot Synthesis, Characterization, and Enhanced Photocatalytic Activity of a BiOBr-Graphene Composite. *Chem. Eur. J.* 18, 14359–14366. doi:10.1002/chem.201200892

Tu, X., Qian, S., Chen, L., and Qu, L. (2015). The Influence of Sn(II) Doping on the Photoinduced Charge and Photocatalytic Properties of BiOBr Microspheres. *J. Mater. Sci.* 50, 4312–4323. doi:10.1007/s10853-015-8983-3

Vadivel, S., Keerthi, P., Vanitha, M., Muthukrishnaraj, A., and Balasubramanian, N. (2014). Solvothermal Synthesis of Sm-Doped BiOBr/RGO Composite as an Efficient Photocatalytic Material for Methyl orange Degradation. *Mater. Lett.* 128, 287–290. doi:10.1016/j.matlet.2014.04.047

Vinoth, S., and Pandikumar, A. (2021). Ni Integrated S-gC3N4/BiOBr Based Type-II Heterojunction as a Durable Catalyst for Photoelectrochemical Water Splitting. *Renew. Energ.* 173, 507–519. doi:10.1016/j.renene.2021.03.121

Vinoth, S., Rajaitha, P. M., and Pandikumar, A. (2021). Modulating Photoelectrochemical Water Splitting Performance by Constructing a Type-II Heterojunction between G-C3n4 and BiOI. *New J. Chem.* 45, 2010–2018. doi:10.1039/d0nj05384h

Wang, C.-Y., Zhang, X., Qiu, H.-B., Huang, G.-X., and Yu, H.-Q. (2017). Bi24O31Br10 Nanosheets with Controllable Thickness for Visible-Light-Driven Catalytic Degradation of Tetracycline Hydrochloride. *Appl. Catal. B: Environ.* 205, 615–623. doi:10.1016/j.apcatb.2017.01.015

Wang, F., Gu, Y., Yang, Z., Xie, Y., Zhang, J., Shang, X., et al. (2018). The Effect of Halogen on BiOX (X = Cl, Br, I)/Bi2WO6 Heterojunction for Visible-Light-Driven Photocatalytic Benzyl Alcohol Selective Oxidation. *Appl. Catal. A: Gen.* 567, 65–72. doi:10.1016/j.apcata.2018.09.010

Wang, H., Liao, B., Lu, T., Ai, Y., and Liu, G. (2020). Enhanced Visible-Light Photocatalytic Degradation of Tetracycline by a Novel Hollow BiOCl@CeO2 Heterostructured Microspheres: Structural Characterization and Reaction Mechanism. *J. Hazard. Mater.* 385, 121552. doi:10.1016/j.jhazmat.2019.121552

Wang, J.-J., Zhai, X.-Y., Zhang, G.-Y., Zhang, J.-B., and Zhao, Y.-F. (2020). Facile Construction of BiOBr/Bi2O2CO3 P-N Heterojunction by Precipitation Conversion at Ambient Temperature for Charge Transfer and Photocatalytic Activity. *Solid State. Sci.* 105, 106288. doi:10.1016/j.solidstatesciences.2020.106288

Wang, J., Wei, Y., Yang, B., Wang, B., Chen, J., and Jing, H. (2019). *In Situ* grown Heterojunction of Bi2WO6/BiOCl for Efficient Photoelectrocatalytic CO2 Reduction. *J. Catal.* 377, 209–217. doi:10.1016/j.jcat.2019.06.007

Wang, J., and Zhang, Z. (2020). Co-precipitation Synthesis and Photocatalytic Properties of BiOCl Microflowers. *Optik* 204, 164149. doi:10.1016/j.ijleo.2019.164149

Wang, Q., Liu, Z., Liu, D., Wang, W., Zhao, Z., Cui, F., et al. (2019). Oxygen Vacancy-Rich Ultrathin Sulfur-Doped Bismuth Oxybromide Nanosheet as a Highly Efficient Visible-Light Responsive Photocatalyst for Environmental Remediation. *Chem. Eng. J.* 360, 838–847. doi:10.1016/j.cej.2018.12.038

Wang, S., Yang, X., Zhang, X., Ding, X., Yang, Z., Dai, K., et al. (2017). A Plate-On-Plate Sandwiched Z-Scheme Heterojunction Photocatalyst: BiOBr-Bi 2 MoO 6 with Enhanced Photocatalytic Performance. *Appl. Surf. Sci.* 391, 194–201. doi:10.1016/j.apsusc.2016.07.070

Wang, Y., Jin, J., Chu, W., Cahen, D., and He, T. (2018). Synergistic Effect of Charge Generation and Separation in Epitaxially Grown BiOCl/Bi2S3 Nano-Heterostructure. *ACS Appl. Mater. Inter.* 10, 15304–15313. doi:10.1021/acsami.8b03390

Wang, Z., Chen, M., Huang, D., Zeng, G., Xu, P., Zhou, C., et al. (2019). Multiply Structural Optimized Strategies for Bismuth Oxyhalide Photocatalysis and Their Environmental Application. *Chem. Eng. J.* 374, 1025–1045. doi:10.1016/j.cej.2019.06.018

Wei, Z., Dong, X., Zheng, N., Wang, Y., Zhang, X., and Ma, H. (2020). Novel Visible-Light Irradiation Niobium-Doped BiOBr Microspheres with Enhanced Photocatalytic Performance. *J. Mater. Sci.* 55, 16522–16532. doi:10.1007/s10853-020-05265-3

Weng, B., Liu, S., Zhang, N., Tang, Z.-R., and Xu, Y.-J. (2014a). A Simple yet Efficient Visible-Light-Driven CdS Nanowires-Carbon Nanotube 1D-1D Nanocomposite Photocatalyst. *J. Catal.* 309, 146–155. doi:10.1016/j.jcat.2013.09.013

Weng, B., Xu, F., and Xu, J. (2014b). Hierarchical Structures Constructed by BiOX (X= Cl, I) Nanosheets on CNTs/carbon Composite Fibers for Improved Photocatalytic Degradation of Methyl orange. *J. Nanopart. Res.* 16, 1–13. doi:10.1007/s11051-014-2766-7

WHO/UNICEF Joint Monitoring Programme for Water Supply and Sanitation, UNICEF (2005). *Water for Life: Making it Happen*. Geneva: World health organization.

Wu, D., Yue, S., Wang, W., An, T., Li, G., Yip, H. Y., et al. (2016). Boron Doped BiOBr Nanosheets with Enhanced Photocatalytic Inactivation of *Escherichia coli*. *Appl. Catal. B: Environ.* 192, 35–45. doi:10.1016/j.apcatb.2016.03.046

Wu, H., Yuan, C., Chen, R., Wang, J., Dong, F., Li, J., et al. (2020). Mechanisms of Interfacial Charge Transfer and Photocatalytic NO Oxidation on BiOBr/SnO2 P-N Heterojunctions. *ACS Appl. Mater. Inter.* 12, 43741–43749. doi:10.1021/acsami.0c12628

Wu, H., Zhou, P., Alagarasan, J. K., Jing, J., Zhou, T., and Xu, Y. (2021). Construction of Novel PTh-BiOBr Composite with Enhanced Photocatalytic Degradation of Bisphenol A. *Adv. Powder. Technol.* 32 (7), 2390–2397. doi:10.1016/j.apt.2021.05.022

Wu, X., Ng, Y. H., Wang, L., Du, Y., Dou, S. X., Amal, R., et al. (2017). Improving the Photo-Oxidative Capability of BiOBr via crystal Facet Engineering. *J. Mater. Chem. A.* 5, 8117–8124. doi:10.1039/c6ta10964k

Xia, J., Ji, M., Li, W., Di, J., Xu, H., He, M., et al. (2016). Synthesis of Erbium Ions Doped BiOBr via a Reactive Ionic Liquid with Improved Photocatalytic Activity. *Colloids Surf. A: Physicochemical Eng. Aspects* 489, 343–350. doi:10.1016/j.colsurfa.2015.10.037

Xiang, Y., Ju, P., Wang, Y., Sun, Y., Zhang, D., and Yu, J. (2016). Chemical Etching Preparation of the Bi2WO6/BiOI P-N Heterojunction with Enhanced Photocatalytic Antifouling Activity under Visible Light Irradiation. *Chem. Eng. J.* 288, 264–275. doi:10.1016/j.cej.2015.11.103

Xiao, W., Su, Y., Luo, J., Jiang, L., Wu, X., Liu, Z., et al. (2020). Flower-like Hierarchical Architecture of BiOI/ZnO P-N junction Composites with High-Efficient Visible-Light Photodegradation Activities. *Solid State. Sci.* 108, 106432. doi:10.1016/j.solidstatesciences.2020.106432

Xiao, X., and Zhang, W.-D. (2010). Facile Synthesis of Nanostructured BiOI Microspheres with High Visible Light-Induced Photocatalytic Activity. *J. Mater. Chem.* 20, 5866–5870. doi:10.1039/c0jm00333f

Xie, Y., Kocaefe, D., Chen, C., and Kocaefe, Y. (2016). Review of Research on Template Methods in Preparation of Nanomaterials. *J. Nanomater.* 2016, 1–10. doi:10.1155/2016/2302595

Xiong, J., Cheng, G., Lu, Z., Tang, J., Yu, X., and Chen, R. (2011a). BiOCOOH Hierarchical Nanostructures: Shape-Controlled Solvothermal Synthesis and Photocatalytic Degradation Performances. *CrystEngComm* 13, 2381–2390. doi:10.1039/c0ce00705f

Xiong, J., Cheng, G., Li, G., Qin, F., and Chen, R. (2011b). Well-crystallized Square-like 2D BiOCl Nanoplates: Mannitol-Assisted Hydrothermal Synthesis and Improved Visible-Light-Driven Photocatalytic Performance. *RSC Adv.* 1, 1542–1553. doi:10.1039/c1ra00335f

Xiong, J., Di, J., and Li, H. (2018). Atomically Thin 2D Multinary Nanosheets for Energy-Related Photo, Electrocatalysis. *Adv. Sci.* 5, 1800244. doi:10.1002/advs.201800244

Xiong, J., Song, P., Di, J., and Li, H. (2020). Bismuth-rich Bismuth Oxyhalides: a New Opportunity to Trigger High-Efficiency Photocatalysis. *J. Mater. Chem. A.* 8, 21434–21454. doi:10.1039/d0ta06044e

Xiong, X., Ding, L., Wang, Q., Li, Y., Jiang, Q., and Hu, J. (2016). Synthesis and Photocatalytic Activity of BiOBr Nanosheets with Tunable Exposed {0 1 0} Facets. *Appl. Catal. B: Environ.* 188, 283–291. doi:10.1016/j.apcatb.2016.02.018

Xue, X., Chen, R., Chen, H., Hu, Y., Ding, Q., Liu, Z., et al. (2018). Oxygen Vacancy Engineering Promoted Photocatalytic Ammonia Synthesis on Ultrathin Two-Dimensional Bismuth Oxybromide Nanosheets. *Nano Lett.* 18, 7372–7377. doi:10.1021/acs.nanolett.8b03655

Yadav, M., Garg, S., Chandra, A., Gläser, R., and Hernadi, K. (2020). Green BiOI Impregnated 2-dimensional Cylindrical Carbon Block: A Promising Solution for Environmental Remediation and Easy Recovery of the Photocatalyst. *Separat. Purif. Techn.* 240, 116628. doi:10.1016/j.seppur.2020.116628

Yadav, M., Garg, S., Chandra, A., and Hernadi, K. (2019). Immobilization of green BiOX (X= Cl, Br and I) Photocatalysts on Ceramic Fibers for Enhanced Photocatalytic Degradation of Recalcitrant Organic Pollutants and Efficient Regeneration Process. *Ceramics Int.* 45, 17715–17722. doi:10.1016/j.ceramint.2019.05.340

Yadav, M., Garg, S., Chandra, A., Jyoti, P. P., Ingole, P. P., Bardos, E., et al. (2021). Quercetin-mediated 3-D Hierarchical BiOI-Q and BiOI-Q-Ag Nanostructures with Enhanced Photodegradation Efficiency. *J. Alloys Compd.* 856, 156812. doi:10.1016/j.jallcom.2020.156812

Yan, X., Zhao, H., Li, T., Zhang, W., Liu, Q., Yuan, Y., et al. (2019). *In Situ* synthesis of BiOCl Nanosheets on Three-Dimensional Hierarchical Structures for Efficient Photocatalysis under Visible Light. *Nanoscale* 11, 10203–10208. doi:10.1039/c9nr02304f

Yang, H. (2021). A Short Review on Heterojunction Photocatalysts: Carrier Transfer Behavior and Photocatalytic Mechanisms. *Mater. Res. Bull.* 142, 111406. doi:10.1016/j.materresbull.2021.111406

Yang, J., Wang, X., Lv, X., Xu, X., Mi, Y., and Zhao, J. (2014). Preparation and Photocatalytic Activity of BiOX-TiO2 Composite Films (X=Cl, Br, I). *Ceramics Int.* 40, 8607–8611. doi:10.1016/j.ceramint.2014.01.077

Yang, L., Chen, J., Liu, X., Que, M., Zhao, Y., Zheng, H., et al. (2021). 2D/2D BiOBr/(001)-TiO2 Heterojunction toward Enhanced Photocatalytic Degradation Activity of Rhodamine B. *J. Alloys Compd.* 884, 161064. doi:10.1016/j.jallcom.2021.161064

Yang, W., Wen, Y., Chen, R., Zeng, D., and Shan, B. (2014). Study of Structural, Electronic and Optical Properties of Tungsten Doped Bismuth Oxychloride by DFT Calculations. *Phys. Chem. Chem. Phys.* 16, 21349–21355. doi:10.1039/c4cp02801e

Yang, Y., Zhang, C., Lai, C., Zeng, G., Huang, D., Cheng, M., et al. (2018). BiOX (X = Cl, Br, I) Photocatalytic Nanomaterials: Applications for Fuels and Environmental Management. *Adv. Colloid Interf. Sci.* 254, 76–93. doi:10.1016/j.cis.2018.03.004

Yao, S., Wang, J., Zhou, X., Zhou, S., Pu, X., and Li, W. (2020). One-pot Low-Temperature Synthesis of BiOX/TiO2 Hierarchical Composites of Adsorption Coupled with Photocatalysis for Quick Degradation of Colored and Colorless Organic Pollutants. *Adv. Powder Techn.* 31, 1924–1932. doi:10.1016/j.apt.2020.02.023

Yao, W., Wang, H., Xu, X. H., Zhou, J. T., Yang, X. N., Zhang, Y., et al. (2004). Photocatalytic Property of Bismuth Titanate Bi2Ti2O7. *Appl. Catal. A: Gen.* 259, 29–33. doi:10.1016/j.apcata.2003.09.004

Ye, L., Su, Y., Jin, X., Xie, H., and Zhang, C. (2014). Recent Advances in BiOX (X = Cl, Br and I) Photocatalysts: Synthesis, Modification, Facet Effects and Mechanisms. *Environ. Sci. Nano* 1, 90–112. doi:10.1039/c3en00098b

Ye, L., Tian, L., Peng, T., and Zan, L. (2011). Synthesis of Highly Symmetrical BiOI Single-crystal Nanosheets and Their {001} Facet-dependent Photoactivity. *J. Mater. Chem.* 21, 12479–12484. doi:10.1039/c1jm11005e

Yin, S., Fan, W., Di, J., Wu, T., Yan, J., He, M., et al. (2017). La3+ Doped BiOBr Microsphere with Enhanced Visible Light Photocatalytic Activity. *Colloids Surf. A: Physicochemical Eng. Aspects* 513, 160–167. doi:10.1016/j.colsurfa.2016.10.012

Yu, C.-L., Cao, F.-F., Shu, Q., Bao, Y.-L., Xie, Z.-P., Yu, J., et al. (2012). Preparation, Characterization and Photocatalytic Performance of Ag/BiOX (X= Cl, Br, I) Composite Photocatalysts. *Acta Phys-chim. Sin.* 28, 647–653. doi:10.3866/PKU.WHXB201201051

Yu, C., Cao, F., Li, G., Wei, R., Yu, J. C., Jin, R., et al. (2013). Novel noble Metal (Rh, Pd, Pt)/BiOX(Cl, Br, I) Composite Photocatalysts with Enhanced Photocatalytic Performance in Dye Degradation. *Separat. Purif. Techn.* 120, 110–122. doi:10.1016/j.seppur.2013.09.036

Yu, C., Fan, C., Meng, X., Yang, K., Cao, F., and Li, X. (2011). A Novel Ag/BiOBr Nanoplate Catalyst with High Photocatalytic Activity in the Decomposition of Dyes. *Reac Kinet Mech. Cat* 103, 141–151. doi:10.1007/s11144-011-0291-6

Yu, C., Zhou, W., Yu, J., Cao, F., and Li, X. (2012). Thermal Stability, Microstructure and Photocatalytic Activity of the Bismuth Oxybromide Photocatalyst. *Chin. J. Chem.* 30, 721–726. doi:10.1002/cjoc.201280018

Yu, H., Cao, C., Wang, X., and Yu, J. (2017). Ag-modified BiOCl Single-crystal Nanosheets: Dependence of Photocatalytic Performance on the Region-Selective Deposition of Ag Nanoparticles. *J. Phys. Chem. C* 121, 13191–13201. doi:10.1021/acs.jpcc.7b03213

Yu, H., Huang, B., Wang, H., Yuan, X., Jiang, L., Wu, Z., et al. (2018). Facile Construction of Novel Direct Solid-State Z-Scheme AgI/BiOBr Photocatalysts for Highly Effective Removal of Ciprofloxacin under Visible Light Exposure: Mineralization Efficiency and Mechanisms. *J. Colloid Interf. Sci.* 522, 82–94. doi:10.1016/j.jcis.2018.03.056

Yu, J., and Kudo, A. (2006). Effects of Structural Variation on the Photocatalytic Performance of Hydrothermally Synthesized BiVO4. *Adv. Funct. Mater.* 16, 2163–2169. doi:10.1002/adfm.200500799

Yu, J., Wang, W., and Cheng, B. (2010). Synthesis and Enhanced Photocatalytic Activity of a Hierarchical Porous Flowerlike P-N Junction NiO/TiO2 Photocatalyst. *Chem. Asian J.* 5, 2499–2506. doi:10.1002/asia.201000550

Zhang, C., and Zhu, Y. (2005). Synthesis of Square Bi2WO6 Nanoplates as High-Activity Visible-Light-Driven Photocatalysts. *Chem. Mater.* 17, 3537–3545. doi:10.1021/cm0501517

Zhang, D., Su, C., Yao, S., Li, H., Pu, X., and Geng, Y. (2020). Facile *In Situ* Chemical Transformation Synthesis, Boosted Charge Separation, and Increased Photocatalytic Activity of BiPO4/BiOCl P-N Heterojunction Photocatalysts under Simulated Sunlight Irradiation. *J. Phys. Chem. Sol.* 147, 109630. doi:10.1016/j.jpcs.2020.109630

Zhang, H., Tee, J. C. L., Jaenicke, S., Gondal, M. A., Dastageer, M. A., Basheer, C., et al. (2021). BiOBrnI1-n Solid Solutions as Versatile Photooxidation Catalysts for Phenolics and Endocrine Disrupting Chemicals. *Catal. Today* 375, 547–557. doi:10.1016/j.cattod.2020.01.009

Zhang, K., Liu, C., Huang, F., Zheng, C., and Wang, W. (2006). Study of the Electronic Structure and Photocatalytic Activity of the BiOCl Photocatalyst. *Appl. Catal. B: Environ.* 68, 125–129. doi:10.1016/j.apcatb.2006.08.002

Zhang, K., Zhang, D., Liu, J., Ren, K., Luo, H., Peng, Y., et al. (2012). A Novel Nanoreactor Framework of Iodine-Incorporated BiOCl Core-Shell Structure: Enhanced Light-Harvesting System for Photocatalysis. *CrystEngComm* 14, 700–707. doi:10.1039/c1ce05755c

Zhang, L.-W., Wang, Y.-J., Cheng, H.-Y., Yao, W.-Q., and Zhu, Y.-F. (2009). Synthesis of Porous Bi2WO6Thin Films as Efficient Visible-Light-Active Photocatalysts. *Adv. Mater.* 21, 1286–1290. doi:10.1002/adma.200801354

Zhang, L., Xu, T., Zhao, X., and Zhu, Y. (2010). Controllable Synthesis of Bi2MoO6 and Effect of Morphology and Variation in Local Structure on Photocatalytic Activities. *Appl. Catal. B: Environ.* 98, 138–146. doi:10.1016/j.apcatb.2010.05.022

Zhang, W., Fu, J., Wang, Y., Zhang, X., and Li, J. (2019). A Facile Solvothermal Method Synthesis of Nitrogen-Doped Graphene Quantum dots/BiOX (X=Br,

Cl) Hybrid Material for Enhanced Visible-Light Photoactivity. *Optik* 176, 448–456. doi:10.1016/j.ijleo.2018.08.085

Zhang, W., Zhang, Q., and Dong, F. (2013). Visible-Light Photocatalytic Removal of NO in Air over BiOX (X = Cl, Br, I) Single-Crystal Nanoplates Prepared at Room Temperature. *Ind. Eng. Chem. Res.* 52, 6740–6746. doi:10.1021/ie400615f

Zhang, X., Ai, Z., Jia, F., and Zhang, L. (2008). Generalized One-Pot Synthesis, Characterization, and Photocatalytic Activity of Hierarchical BiOX (X = Cl, Br, I) Nanoplate Microspheres. *J. Phys. Chem. C* 112, 747–753. doi:10.1021/jp077471t

Zhang, Y., Sun, A., Xiong, M., Macharia, D. K., Liu, J., Chen, Z., et al. (2021). TiO2/BiOI P-N junction-decorated Carbon Fibers as Weavable Photocatalyst with UV-Vis Photoresponsive for Efficiently Degrading Various Pollutants. *Chem. Eng. J.* 415, 129019. doi:10.1016/j.cej.2021.129019

Zhang, Y., Wang, Q., Liu, D., Wang, Q., Li, T., and Wang, Z. (2020a). Cu2O-BiOI Isotype (P-p) Heterojunction: Boosted Visible-Light-Driven Photoelectrochemical Activity for Non-enzymatic H2O2 Sensing. *Appl. Surf. Sci.* 521, 146434. doi:10.1016/j.apsusc.2020.146434

Zhang, Y., Shao, Q., Jiang, H., Liu, L., Wu, M., Lin, J., et al. (2020b). One-step Co-precipitation Synthesis of Novel BiOCl/CeO2composites with Enhanced Photodegradation of Rhodamine B. *Inorg. Chem. Front.* 7, 1345–1361. doi:10.1039/c9qi01524h

Zhang, Z., Wang, B., Guo, J., He, Y., Song, P., and Wang, R. (2019). *In Situ* Synthesis of C-Doped BiOBr Micron-Flower by Structural Induction of Sodium Alginate for Rapid Removal Tetracycline. *ChemistrySelect* 4, 14007–14011. doi:10.1002/slct.201903827

Zhao, H., Liu, X., Dong, Y., Xia, Y., Wang, H., and Zhu, X. (2020). Fabrication of a Z-Scheme {001}/{110} Facet Heterojunction in BiOCl to Promote Spatial Charge Separation. *ACS Appl. Mater. Inter.* 12, 31532–31541. doi:10.1021/acsami.0c08687

Zhao, K., Zhang, L., Wang, J., Li, Q., He, W., and Yin, J. J. (2013). Surface Structure-dependent Molecular Oxygen Activation of BiOCl Single-Crystalline Nanosheets. *J. Am. Chem. Soc.* 135, 15750–15753. doi:10.1021/ja4092903

Zhao, L., Zhang, X., Fan, C., Liang, Z., and Han, P. (2012). First-principles Study on the Structural, Electronic and Optical Properties of BiOX (X=Cl, Br, I) Crystals. *Physica B: Condensed Matter* 407, 3364–3370. doi:10.1016/j.physb.2012.04.039

Zhong, S., Wang, X., Wang, Y., Zhou, F., Li, J., Liang, S., et al. (2020). Preparation of Y3+-Doped BiOCl Photocatalyst and its Enhancing Effect on Degradation of Tetracycline Hydrochloride Wastewater. *J. Alloys Compd.* 843, 155598. doi:10.1016/j.jallcom.2020.155598

Zhou, J., Zhou, J., Hu, Z., and Wang, L. (2019). Enhancement of Adsorption and Visible Light Photocatalytic Activity of the Zn2+-Doped BiOBr/PVP Modified Microspheres for RhB. *Mater. Sci. Semiconductor Process.* 90, 112–119. doi:10.1016/j.mssp.2018.10.012

Zhou, S., Shi, T., Chen, Z., Kilin, D., Shui, L., Jin, M., et al. (2019). First-Principles Study of Optoelectronic Properties of the Noble Metal (Ag and Pd) Doped BiOX (X = F, Cl, Br, and I) Photocatalytic System. *Catalysts* 9, 198. doi:10.3390/catal9020198

Zhu, G., Hojamberdiev, M., Zhang, S., Din, S. T. U., and Yang, W. (2019). Enhancing Visible-Light-Induced Photocatalytic Activity of BiOI Microspheres for NO Removal by Synchronous Coupling with Bi Metal and Graphene. *Appl. Surf. Sci.* 467-468, 968–978. doi:10.1016/j.apsusc.2018.10.246

Conflict of Interest: The authors declare that the research was conducted in the absence of any commercial or financial relationships that could be construed as a potential conflict of interest.

Publisher's Note: All claims expressed in this article are solely those of the authors and do not necessarily represent those of their affiliated organizations, or those of the publisher, the editors, and the reviewers. Any product that may be evaluated in this article, or claim that may be made by its manufacturer, is not guaranteed or endorsed by the publisher.